# Atlantic water inflow and sea ice distribution in the northern Barents Sea: A Holocene palaeoceanographic evolution

**Berben SMP[a], Husum K[b], Navarro-Rodriguez A[c], Belt ST[c] and Aagaard-Sørensen S[a]**
[a]Department of Geology, University of Tromsø, N-9037 Tromsø, Norway
[b]Norwegian Polar Institute, Fram Centre, N-9296 Tromsø, Norway
[c]Biogeochemistry Research Centre, School of Geography, Earth and Environmental Sciences, University of Plymouth, Drake Circus, Plymouth PL4 8AA, UK

Correspondence to: Berben SMP (sarah.m.berben@uit.no)

**Keywords:** Atlantic water inflow, sea ice distribution, northern Barents Sea, Holocene, planktic foraminifera, stable isotopes, sea ice biomarkers

## Abstract

We carried out a multi-proxy analysis on a marine sediment core retrieved from the Olga Basin in the northern Barents Sea in order to investigate the interactions between, and variations in, Atlantic water inflow and sea ice distribution throughout the Holocene. This was achieved by analysing planktic foraminifera and their preservation indicators, foraminiferal stable isotopes ($\delta^{18}O$, $\delta^{13}C$) and biomarkers. The resulting sub-centennial records suggest that the early Holocene (ca. 9500 – 5800 cal yr BP) was characterised by short spring seasons and long productive summers. A strong influence of Atlantic water caused an increased heat flux which led to an active ocean feedback mechanism and hence, contributed to a reduced sea ice extent. The Holocene Thermal Optimum was recorded at different time intervals between ca. 9300 and 5800 cal yr BP indicating a proxy-specific response. Throughout the mid Holocene (ca. 5800 – 2200 cal yr BP), the sea ice edge migrated southwards and an overall cooling trend is consistent with reduced summer insolation which affected the sea surface conditions, in particular. During the late Holocene (ca. 2200 – 0 cal yr BP), the different proxies indicate a sub-surface warming, with increased Atlantic water inflow, and sea surface cooling, with extended sea ice cover, likely due to a decoupling between the ocean and the atmosphere. Longer spring seasons and shorter summers were reflected by the most extended sea ice distribution within the entire record. The generally more unstable palaeoceanographic conditions in the late Holocene are attributed to more pronounced positive NAO-like conditions.

## 1 Introduction

The Barents Sea is a relatively small and shallow sea, yet it plays a crucial role in the Arctic climate system, in part, because of significant heat exchange between the ocean and the atmosphere (Serreze et al., 2007). Oceanic heat is brought into the Barents Sea via the inflow of warm Atlantic water and, due to shallow depths, heat loss to the atmosphere is very efficient. Further, it has been suggested that ocean advection strongly influences sea ice extent in the Barents Sea, so the region is central to understanding ocean-sea ice-atmosphere interactions Vinje (2001).

Recently, many Arctic regions have experienced a sharp decline in sea ice cover, and this is most pronounced in the northern Barents Sea (Screen and Simmonds, 2010). Variations in sea

ice within the Barents Sea have been attributed to several different processes (e.g. atmospheric circulation variability, local wind patterns, ice import), although the role of oceanic heat advection is often emphasized as one of the most important factors. For example, Årthun et al. (2012) have argued that recent increases in Atlantic water inflow has resulted in so-called 'Atlantification' of the Barents Sea and this has contributed to a further decline in sea ice cover.

As the impacts of Arctic amplification and the associated sea ice decline reach far beyond the Arctic region (e.g. the link between recent Arctic sea ice loss and continental winter cooling (Yang and Christensen, 2012)), it is clearly necessary to better understand the interaction between Atlantic water inflow and sea ice production, together with any natural variability that occurs over longer timeframes. Instrumental records of past climate variations in the Barents Sea reach back only ca. 100 years (Smedsrud et al., 2013), so longer term records of sea ice and water mass distribution need to be derived from proxy records. Previous proxy records from the northern Barents Sea (e.g. Duplessy et al., 2001; Lubinski et al., 2001; Risebrobakken et al., 2011; Klitgaard Kristensen et al., 2013), the western Barents Sea (Berben et al., 2014) and the Svalbard margin (e.g. Slubowska et al., 2005; Rasmussen et al., 2007; Spielhagen et al., 2011; Müller et al., 2012; Werner et al., 2013) have demonstrated various fluctuations in both the influence of Atlantic water inflow and in sea ice distribution throughout the Holocene.

During the early Holocene, the so-called Holocene Thermal Maximum (HTM) has been identified in numerous previous studies and has been linked, primarily, to an increase in solar insolation and further to factors such as land-cover feedbacks and coupled atmospheric-oceanic dynamics; especially the northward penetration of relatively warm Atlantic water (e.g. Berger, 1978; Koç et al., 1993; Kaufman et al., 2004). For example, the HTM has been observed through increased sea surface temperatures (SST) and enhanced Atlantic water inflow (e.g. Duplessy et al., 2001; Sarnthein et al., 2003; Hald et al., 2007; Risebrobakken et al., 2010) along the Norwegian coast (e.g. Husum and Hald, 2004) and the Svalbard margin (e.g. Slubowska et al., 2005; Slubowska-Woldengen et al., 2007; Werner et al., 2013). The apparent timing of the HTM varies, however, possibly as a result of variable location and the depth habitat and/or response time of the different proxies to atmospheric changes (e.g. due to increased insolation), which underscores the influencing role of the interaction between the atmosphere and the ocean (Kaufman et al., 2004; Moros et al., 2004; Hald et al., 2007). In any case, the HTM was followed by the Neoglacial cooling, a period generally characterized by

the return of cooler conditions in different northern high latitude regions (e.g. Wanner et al., 2008). Marine proxy records generally show reduced SST records, a dominance of Arctic water and increased sea ice, consistent with decreasing summer insolation at high latitudes such as in the Barents Sea (e.g. Duplessy et al., 2001; Sarnthein et al., 2003; Hald et al., 2007; Risebrobakken et al., 2010; Klitgaard Kristensen et al., 2013) and the Svalbard margin (e.g. Rasmussen et al., 2007; Müller et al., 2012; Rasmussen et al., 2012; Werner et al., 2013).

During the Late Holocene, evidence for strengthened Atlantic water inflow has been presented for the Barents Sea (e.g. Duplessy et al., 2001; Lubinski et al., 2001; Berben et al., 2014) and the Svalbard margin (e.g. Slubowska-Woldengen et al., 2007; Jernas et al., 2013; Werner et al., 2013; Zamelczyk et al., 2013), while some air temperature reconstructions, based on terrestrial records from Fennoscandinavia and ice core records from Greenland and Svalbard, indicate an overall cooling (e.g. Dahl-Jensen et al., 1998; Bjune et al., 2009; Kaufman et al., 2009; Divine et al., 2011). The dominance of cold Arctic water and reduced Atlantic water inflow at the western and northern margin of Svalbard has also been identified for the late Holocene from marine records (e.g. Slubowska et al., 2005; Skirbekk et al., 2010).

Here, we combine proxy data from planktic foraminiferal fauna assemblages, stable isotopes ($\delta^{18}O$, $\delta^{13}C$) and biomarkers (including $IP_{25}$ as a sea ice proxy; Belt et al., 2007; Belt and Müller, 2013; Brown et al., 2014) in a marine sediment core obtained from the northern Barents Sea to construct an integrated sub-surface water mass and sea ice record for the Holocene. Today, the study site is influenced by Atlantic derived water masses (Abrahamsen et al., 2006) and is covered by seasonal sea ice (Figure 1). As such, it represents a key location for investigating the palaeoceanographic evolution of Atlantic water inflow and sea ice distribution throughout the Holocene. On the basis of the combined proxy record, we propose different oceanographic scenarios that emphasize the interaction between surface water masses and sea ice distribution, and discuss these further, by comparison with outcomes from previous studies from the region.

## 2 Present day oceanographic setting of the Barents Sea

The Barents Sea is an epicontinental shelf located between the Norwegian-Russian coast, Novaya Zemlya and the Svalbard and Franz Josef Land archipelagos (Figure 1). The northern boundary of the Barents Sea is defined by the Nansen Basin continental slope (Jakobsson et

al., 2004). The Barents Sea is characterized by several water masses and represents a major passage for Atlantic water entering the Arctic Ocean (Carmack et al., 2006).

The Norwegian Atlantic Current (NwAC) brings relatively warm Atlantic water (>2 °C, >35 ‰) towards the high latitude North Atlantic Ocean (Hopkins, 1991) (Figure 1A). Before entering the Barents Sea, the NwAC splits into two different currents: the West Spitsbergen Current (WSC) and the North Cape Current (NCaC) (Figure 1A), both of which are responsible for the transport of warm saline Atlantic water into the Arctic Ocean, in particular the WSC (Aagaard and Greisman, 1975). The WSC continues northwards along the western Barents Sea slope and splits in the Fram Strait into three branches; the Return Atlantic Current (RAC), the Yermak Branch (YB) and the Svalbard Branch (SB) (e.g. Manley, 1995). The latter enters the Arctic Ocean north of Svalbard as a sub-surface current flowing eastward up and beyond the Franz Victoria and St. Anna Troughs. Hence, the Barents Sea becomes influenced by the sub-surface inflow of Atlantic water via the Northern Barents Sea Opening (NBSO) (Figure 1A). Subsequently, Atlantic water is advected south-westwards into the northern Barents Sea and has been observed year-round in the Olga Basin, which is the study site here (Abrahamsen et al., 2006). Further, the northern Barents Sea and, in particular, the Olga Basin, is also influenced by Atlantic water that enters as a submerged flow from the south (e.g. Novitskiy, 1961; Loeng, 1991; Pfirman et al., 1994; Aksenov et al., 2010). This Atlantic water is brought to the area by the NCaC which flows northwards via the Barents Sea Opening (BSO) into the southern Barents Sea and parallel to the coastal current system (Loeng, 1991; Loeng et al., 1993; Midttun, 1985; Rudels, 1987) (Figure 1A). Finally, after mixing and heat loss, Atlantic water leaves the Barents Sea through the Barents Sea Exit (BSX) and reaches the Arctic Ocean via the St. Anna Trough (e.g. Schauer et al., 2002) (Figure 1A). South of the NCaC, the Norwegian Coastal Current (NCC) transports Coastal water (2 - 13 °C, 32 - 35 ‰) along the Norwegian and northern Russian coasts (Hopkins, 1991) (Figure 1A). Polar water (0 - 2 °C, 33 - 33.4 ‰) is brought from the Arctic Ocean into the Barents Sea through the Franz Victoria and St. Anna Troughs, via the East Spitsbergen Current (ESC) and the Bear Island Current (BIC), respectively (Hopkins, 1991) (Figure 1A).

In contrast to the Atlantic water dominated southern Barents Sea, the northern Barents Sea is dominated by Arctic water (~0.5 °C, ~34.8 ‰) and is characterized by reduced temperature and salinity, as well as seasonal sea ice cover (Hopkins, 1991). Arctic water is formed when relatively warm Atlantic water converges and merges with cold, less saline and ice loaded Polar water. Hence, temperature and salinity values progressively decrease towards the north-

eastern Barents Sea resulting in what is classified as Atlantic derived water (>0 °C, >34.75 ‰) (Gammelsrød et al., 2009). Further, in the north-eastern Barents Sea, extensive sea ice formation, brine rejection in winter and the subsequent melting of sea ice in summer, lead to a stable and strong stratification (Wassmann et al., 2006). A small fraction of Atlantic water in the northern Barents Sea enters the area from the north as a sub-surface flow and is located below Arctic water. The majority of Atlantic water entering the region from the south is cooled due to a strong heat loss to the atmosphere, but retains high salinity. As a result, the latter, denser water mass flows below the Atlantic water mass advected from the north (Pfirman et al., 1994). Finally, dense and cold deep waters are formed through cooling and salt rejection during sea ice growth. The Barents Sea is an important contributor for the production and export of dense water into the Arctic Ocean and thereby plays a central role in the global ocean circulation and climate (Årthun et al., 2011).

The fronts dividing these different water masses are one of the main oceanographic features of the near-surface waters of the Barents Sea (Pfirman et al., 1994). Defined as a sharp climatic gradient in terms of temperature, salinity and sea ice coverage, the Polar and Arctic Fronts are the respective boundaries between Polar/Arctic and Arctic/Atlantic waters. These are closely related to the overall distribution of sea ice, in particular, and the average winter and summer sea ice margins (Vinje, 1977). Although sea ice advection from the Arctic Ocean does occur, sea ice is mainly formed locally during fall and winter (Loeng, 1991). The sea ice edge divides the Barents Sea into two different oceanographic areas, each with their own characteristics (Figure 1B). The sea ice extent is regulated by the inflow of Atlantic water into the western Barents Sea, which sets the boundary of the mainly ice-free Atlantic domain in the south-western Barents Sea (Årthun et al., 2012). In contrast, the north-eastern Barents Sea experiences large changes in seasonal sea ice distribution (Vinje, 2001; Sorteberg and Kvingedal, 2006) with maximum sea ice extent during March/April and minimum cover occurring throughout August/September (Figure 1B). Further, annual variability during recent decades might be explained by cyclone activity causing fluctuations in sea ice transport, to and from the Arctic Ocean into the north-eastern Barents Sea (Kwok et al., 2005; Sorteberg and Kvingedal, 2006; Ellingsen et al., 2009; Kwok, 2009). The interplay among the different water masses and other influences over sea ice formation determine the position of the marginal ice zone (MIZ), an area characterized by its high surface productivity during the summer season (e.g. Smith and Sakshaug, 1990). Within the Barents Sea, the major part of the biological primary production results from a peak algal bloom along the ice edge during

the spring as sea ice retreats (Sakshaug et al., 1992). Consequently, the Barents Sea is one of the most productive areas of the Arctic Seas (Wassmann et al., 2006).

# 3 Material and methods

A 245 cm long marine sediment core NP05-11-70GC was retrieved in 2005 by the RV *Lance* south of Kong Karls Land (Olga Basin) within the northern Barents Sea (78.40° N, 32.42° E; 293 m water depth) (Figure 1). A CTD profile taken at the same location illustrates the presence of Arctic water at the surface, with Atlantic water below ca. 150 m (Figure 2). Only the upper section of the core (0 - 124.5 cm; 1-cm intervals) was investigated in the current study.

## 3.1 Chronology

A depth-age model for NP05-11-70GC was developed using linear interpolation between three calibrated AMS $^{14}$C dates obtained from benthic foraminifera and the assumption that the core top represents 0 cal yr BP (Figure 3). The AMS $^{14}$C dates were calibrated using Calib 6.1.1 (Stuiver and Reimer, 1993) and the Marine09 calibration curve (Reimer et al., 2009). A local reservoir age ($\Delta$R) of 105 ± 24 was indicated for the Svalbard area by Mangerud et al. (2006) and subsequently used in the calibration (Table 1). The resulting depth-age model ranges between 0 and 9417 cal yr BP (Figure 3). The sedimentation rates vary between 0.07 and 0.18 mm/yr, so the sampling resolution is 55 - 134 years (Figure 3).

## 3.2 Planktic foraminifera

Foraminiferal samples were freeze-dried before they were wet-sieved through three different size fractions (1000, 100 and 63 µm) and dried at 40 °C. Planktic foraminiferal assemblages were determined for 123 samples using the 100 - 1000 µm size fraction following Knudsen (1998). Following the recommendations of Forcino (2012), the relative abundances (%) of each species were calculated for samples containing more than 25 specimens (82 samples). The identification of left and right coiling *Neogloboquadrina pachyderma* was achieved following Darling et al. (2006); the left coiling form was identified as *N. pachyderma*, and the

right coiling form was identified as *Neogloboquadrina incompta*, (Cifelli, 1961). The planktic foraminiferal concentrations (#/g sediment) and fluxes (#/cm$^2$/yr) were also calculated; the latter being calculated following Ehrmann and Thiede (1985).

The dissolution of foraminiferal shells was investigated by calculating the mean shell weight (µg) of *N. pachyderma* (Broecker and Clark, 2001; Barker and Elderfield, 2002; Beer et al., 2010) and the fragmentation (%) of foraminiferal tests (Conan et al., 2002). 25 well preserved (visually) and square shaped *N. pachyderma* specimens were picked from a narrow size range (150 - 250 µm) in order to reduce problems of ontogeny and size difference induced variability (Barker et al., 2004). It was possible to obtain a mean weight for 110 samples of *N. pachyderma* using a Mettler Toledo microbalance (0.1 µg sensitivity). The fragmentation of planktic foraminiferal tests was calculated for the 82 samples that contained a total number of >25 specimens within the 100 - 1000 µm size fraction. The fragmentation was calculated using the equation proposed by Pfuhl and Shackleton (2004) (Equation 1).

$$Fragmentation\ (\%) = \frac{\#\ fragments/g}{\#fragments/g/3 + \#\ tests/g} * 100 \qquad \text{[Equation 1]}$$

### 3.3 Stable isotope analysis

Stable isotope ($\delta^{18}O$, $\delta^{13}C$) analyses were performed on the foraminiferal tests of *N. pachyderma*. All specimens were selected from a narrow size range (150 - 250 µm) in order to minimize size dependent effects on isotopic composition (Aksu and Vilks, 1988; Keigwin and Boyle, 1989; Oppo and Fairbanks, 1989; Donner and Wefer, 1994; Bauch et al., 2000). Sufficient specimens were obtained from 105 samples. Samples were analysed using a Finnigan MAT 253 mass spectrometer coupled to an automated Kiel device at the Geological Mass Spectrometer (GMS) Laboratory at the University of Bergen. These measurements were conducted with a reproducibility of ± 0.06 ‰ ($\delta^{18}O$) and ± 0.03 ‰ ($\delta^{13}C$), and data are reported on the ‰ versus VPDB scale calibrated with NBS-19. Corrections for the ice volume effect were applied on the measured $\delta^{18}O$ values according to Fairbanks (1989). No vital effect corrections were applied for the isotope measurements in this study as published estimates of species-specific vital effects are often inconsistent (e.g. Kohfeld et al., 1996; Bauch et al., 1997; Stangeew, 2001; Simstich et al., 2003), possibly due to seasonal changes of the apparent vital effect (Jonkers et al., 2010).

### 3.4 Biomarker analysis

Biomarker analysis was performed on 49 sub-samples (ca. 1 g) providing a centennial resolution. Prior to analysis, sub-samples were freeze-dried and stored at -20 °C. The general methodology was as described previously (Belt et al., 2012; Brown and Belt, 2012) with some modifications. Three internal standards (IS) were added to permit quantification of the biomarkers using gas chromatography-mass spectrometry (GC-MS) (Belt et al., 2012). 9-octylhetadec-8-ene (9-OHD, 10 µL; 1 µg $mL^{-1}$) and 7-hexylnonadecane (7-HND, 10 µL; 1 µg $mL^{-1}$) were added for the quantification of $IP_{25}$, while 5α-androstan-3β-ol (10 µL; 1 µg $mL^{-1}$) was used to quantify brassicasterol. Subsequently, a total organic extract was obtained according to previous descriptions (Belt et al., 2012; Brown and Belt, 2012).

Before fractionation into individual lipid classes, it was necessary to remove elemental sulfur from the TOEs that would otherwise have interfered with the GC-MS analysis. To do this, hexane (1 mL), tetrabutylammonium sulphite (TBA, 1mL) and 2-propanol (1 mL) were added to the TOEs and suspensions were shaken by hand for ca. 1 min. Thereafter, Milli-Q water (3 mL) was added, and mixtures were shaken further (1 min) and centrifuged, after which, the lipid-containing hexane layer was decanted. This procedure was repeated twice more before the hexane was removed using a nitrogen stream. Partially purified TOEs were then separated into non-polar (hexane, 6 mL) and polar fractions (20:80 methylacetate/hexane, 6 mL) using open column chromatography ($SiO_2$). Further separation of the hexane fraction into saturated and unsaturated components was carried out using glass pipettes containing silver ion solid phase extraction (SPE) material (Supelco discovery® Ag-Ion; 100 mg). After conditioning with acetone (3 mL) and hexane (3 mL), saturated (hexane, 1 mL) and unsaturated hydrocarbon fractions (including $IP_{25}$) (acetone, 2 mL) were obtained. Polar fractions containing brassicasterol were derivatized using N,O-Bis(trimethylsilyl)trifluoroacetamide (BSTFA, 50 µL, 70 °C; 1h).

All fractions were analysed using GC-MS with operating conditions as described by Belt et al. (2012). Identification of the lipids of interest was based on their characteristic GC retention times and mass spectra compared with those of reference compounds in total ion current chromatogram (TIC). Quantification of lipids was achieved by comparison of peak area integrations of selected ions with those of the internal standard in selected ion monitoring (SIM) mode (Brown et al., 2011; Belt et al., 2012). These ratios were normalized to instrumental response factors and sediment mass (and total organic carbon content) and also

converted to biomarker fluxes (µg/cm$^2$/yr) (Belt et al., 2012) using the same method described previously for foraminifera. Concentrations of $IP_{25}$ and brassicasterol were also combined to derive the so-called $P_BIP_{25}$ index that has the potential to provide semi-quantitative estimates of sea ice cover (Müller et al., 2011).

# 4 Results and Interpretation

Overall, the different proxies show distinct changes throughout the record time, so they are described here in terms of individual time intervals that reflect the main stages of palaeoceanographic evolution. These intervals are: early Holocene (ca. 9500 – 5800 cal yr BP), mid Holocene (ca. 5800 – 2200 cal yr BP) and late Holocene (ca. 2200 – 0 cal yr BP).

## 4.1 Early Holocene (ca. 9500 – 5800 cal yr BP)

The early Holocene (ca. 9500 – 5800 cal yr BP) is marked by the appearance of polar and subpolar planktic foraminifera, although the absolute abundances and fluxes remain relatively low (<2.46 #/g sediment and <0.04 #/cm$^2$/yr) during the first part of this period (ca. 9500 – 7300 cal yr BP) (Figure 4A; 5A). This could indicate an influence of sea ice at the core site (e.g. Carstens, 1997). Between ca. 7300 and 6500 cal yr BP, there are increases in concentration and flux of foraminifera towards 5.50 #/g sediment and 0.09 #/cm$^2$/yr, respectively, most likely indicating increased influence of Atlantic water (e.g. Johannessen et al., 1994). After ca. 6500 cal yr BP, foraminiferal concentrations and fluxes fall rapidly towards 2.79 #/g sediment and 0.02 #/cm$^2$/yr, respectively.

Within the early Holocene (ca. 9500 – 5800 cal yr BP), the extent of fragmentation falls in the range 14 - 56 % with a mean value of 32 % (Figure 4B). The mean shell weight varies between 5 and 10 µg until ca. 7300 cal yr BP, followed by more consistent values (ca. 7.5 µg) towards ca. 5800 cal yr BP (Figure 4C). Although only a few data points of fragmentation were recorded between ca. 9500 and 7300 cal yr BP, the wide range in both fragmentation and mean shell weight could indicate fluctuating preservation conditions. The relatively high and consistent mean shell weight values between ca. 7300 and 5800 cal yr BP may reflect better preservation conditions, possibly related to an increased influence of Atlantic water. Previously, better calcium carbonate preservation has been associated with increased

production of organic matter in regions of higher Atlantic water input (e.g. Hebbeln et al., 1998; Henrich et al., 2002).

The foraminiferal assemblages in the early Holocene are dominated by *N. pachyderma* (ca. 95 %) (Figure 5B), indicating Arctic conditions at the study site (Volkmann, 2000). Between ca. 7300 and 5800 cal yr BP, the relative abundances of *Turborotalita quinqueloba, N. incompta* and *Globigerinita glutinata* show increased values, up to ca. 24, 27 and 4 %, respectively (Figure 5C-E). These species are associated with subpolar conditions and relatively warm Atlantic (sub-surface) water (Bé and Tolderlund, 1971; Johannessen et al., 1994; Carstens et al., 1997). These foraminiferal fauna changes between ca. 7300 and 5800 cal yr BP are most likely reflecting the HTM at the core site. In addition, *T. quinqueloba* has also been found to be characteristic of Arctic Front conditions in the western Barents Sea (Burhol, 1994), where it responds to a plentiful nutrient supply (Reynolds and Thunnel, 1985; Johannessen et al., 1994).

Studies of recent foraminiferal calcite and the isotopic composition of water masses by Lubinski et al. (2001) demonstrate that, in the Barents Sea, the planktic foraminiferal oxygen isotope signals are controlled mainly by temperature changes, since modern surface water temperatures vary much more than salinity. However, the water masses in the region were also influenced by meltwater and reduced salinities during the very early Holocene, but this influence ended around ca. 11 000 cal yr BP and thus, well before the onset of the current oxygen isotope record (Klitgaard Kristensen et al., 2013). Therefore, it is assumed that the stable oxygen isotope record of the current study is mainly controlled by temperature. During the early Holocene (ca. 9500 – 5800 cal yr BP), the $\delta^{18}O$ record has a value of 3.87 ‰ (Figure 6A). $\delta^{18}O$ values then reduce to ca. 3.78 ‰ towards ca. 8800 cal yr BP, followed by a period (ca. 8800 – 7300 cal yr BP) characterized by more depleted values (ca. 3.58 ‰). This depletion (ca. 0.2 ‰) might indicate a small temperature rise, possibly indicating a gradual shift towards warmer conditions due to increased inflow of Atlantic water. The sharp enrichment in $\delta^{18}O$ between ca. 7600 and 7300 cal yr BP is followed by values that fluctuate around ca. 3.70 ‰ until ca. 5800 cal yr BP. This possibly indicates cooler conditions after ca. 7300 cal yr BP, and that the core site became more influenced by oceanic front conditions. Here, the relatively light $\delta^{18}O$ values between ca. 8800 and 7300 cal yr BP coincide with high insolation values, thus indicating the HTM at the core site (Figure 6). Throughout the early Holocene (ca. 9500 – 5800 cal yr BP), $\delta^{13}C$ values show depletion from 0.37 to 0.01 ‰ between ca. 9500 and 8500 cal yr BP (Figure 6B) consistent with reduced primary production

and/or increased stratification. This trend is reversed at ca. 5800 cal yr BP, with enriched $\delta^{13}C$ values (ca. 0.80 ‰) indicating increased primary production and/or enhanced ventilation (e.g. Spielhagen and Erlenkeuser, 1994) (Figure 6B).

The concentration and flux of the sea ice biomarker $IP_{25}$ (Belt et al., 2007; Belt and Müller, 2013; Brown et al., 2014) shows a rapid decrease (<200 cal yr) at the start of the early Holocene (ca. 9500 – 5800 cal yr BP), whereas those of brassicasterol increase (Figure 7A-B). Consistent with these observations, a reduction in the $P_BIP_{25}$ index from 0.37 to 0.16 also indicates a reduction in sea ice cover with the presence of more open water conditions (Müller et al., 2011) (Figure 7D). From ca. 9300 to 6500 cal yr BP, $IP_{25}$ values increase, but still remain relatively low (ca. 0.05 to 0.10 µg/g OC) (Figure 7A). On the other hand, brassicasterol shows an opposite trend, albeit with some fluctuations around ca. 23 µg/g OC (Figure 7B). Consistent with the foraminiferal assemblages and $\delta^{18}O$ record, these biomarker data also indicate the occurrence of the HTM at the core site throughout the early Holocene. The biomarker data reflects the HTM between ca. 9300 and 6500 cal yr BP, after which, $IP_{25}$ abundances increase, suggesting termination of the HTM. The early Holocene is also characterized by a decreasing trend in TOC, although values remain relatively high (ca. 1.65 to 2.00 %) (Figure 7C). The $P_BIP_{25}$ index shows the lowest values of the record (0.16 - 0.40) suggesting a period characterized by low or variable seasonal sea ice cover and influenced substantially by open water conditions (Müller et al., 2011) (Figure 7D).

### 4.2 Mid Holocene (ca. 5800 – 2200 cal yr BP)

Throughout the mid Holocene (ca. 5800 – 2200 cal yr BP), both planktic foraminiferal concentrations and fluxes show a general increase towards ca. 8.00 #/g sediment and ca. 0.15 #/$cm^2$/yr, respectively (Figure 4A; 5A). The mean shell weight remains relatively stable (ca. 7 µg) with a small decrease towards the end of the interval, whereas the fragmentation record exhibits an overall decrease from ca. 42 to 16 %, indicating improved preservation (Figure 4C-B). The relative abundances of *T. quinqueloba* and *N. incompta* reduce after ca. 5800 cal yr BP and remain relatively stable (ca. 3 - 4 %) towards ca. 2200 cal yr BP (Figure 5C-D). Throughout this period, *N. pachyderma* clearly dominates (ca. 90 %) the planktic foraminiferal fauna (Figure 5B), suggesting a relatively stable period characterized by a dominance of colder Arctic water (Volkmann, 2000).

The $\delta^{18}O$ record remains relatively stable throughout the mid Holocene (ca. 5800 – 2200 cal yr BP) (Figure 6A) with relatively high values (ca. 3.70 ‰) most likely also indicating a decreased influence of Atlantic water. The $\delta^{13}C$ record continues to increase from 0.76 towards 0.90 ‰, indicative of increased ventilation (Spielhagen and Erlenkeuser, 1994) (Figure 6B), although increased $\delta^{13}C$ values might also be attributed to an increase in primary production resulting from a stronger influence of oceanic front conditions.

$IP_{25}$ increases to ca. 0.25 µg/g OC during the mid Holocene (ca. 5800 – 2200 cal yr BP), while brassicasterol shows a decreasing trend to 10 µg/g OC (Figure 7A-B). Combined, the $P_BIP_{25}$ values continue their increasing trend from the early Holocene (0.4 - 0.7) (Figure 7D), reaching values indicative of MIZ conditions according to Müller et al. (2011). As such, the biomarker data indicate a gradual increase in seasonal (spring) sea ice cover, most likely related to the reduced July insolation causing a cooling at the sea surface.

### 4.3 Late Holocene (ca. 2200 – 0 cal yr BP)

During the late Holocene (ca. 2200 – 0 cal yr BP), three episodes of increased values for both planktic foraminiferal concentrations and fluxes are observed between ca. 2200 and 2000 cal yr BP, ca. 1600 and 700 cal yr BP, and ca. 400 and 0 cal yr BP (Figure 4A; 5A). These three episodes show the highest fluxes and concentrations of the entire record (up to 0.16 #/$cm^2$/yr and 10 #/g sediment, respectively). The degree of fragmentation also generally increases (to ca. 50 %), whereas the mean shell weight shows a general decrease towards ca. 4.5 µg (Figure 4B-C). In addition to these general trends, the mean shell weight and, in particular, the planktic foraminiferal fragmentation, show highly fluctuating values (ca. 9 - 83 %) (Figure 4C-B). Despite these fluctuations, however, this interval shows an overall change towards enhanced dissolution. This may be caused by an increased influence of the MIZ and its associated high surface productivity causing a reduced preservation of calcium carbonate (Huber et al., 2000; Scott et al., 2008). Additionally, brine rejection may form corrosive bottom water masses causing dissolution at the sea floor (e.g. Midttun, 1985; Steinsund and Hald, 1994). This has been observed for recent benthic foraminiferal faunas in the Barents Sea (Steinsund and Hald, 1994).

The relative abundance of *N. pachyderma* shows a general decrease towards ca. 65 % suggesting a reduced dominance of Arctic water at the core site (Figure 5B). The

corresponding increasing trend in relative abundances of other species is also seen in their individual fluxes (Figure 5C-G). Thus, in the periods between ca. 2200 – 2000, 1600 – 700 and 400 – 0 cal yr BP, *T. quinqueloba* and *N. incompta* both reach very high abundance and flux values. These changes argue for episodes of enhanced influence of Atlantic water and/or front conditions. After ca. 2000 cal yr BP, increasing values of *G. bulloides* (ca. 8 %) and in particular *G. glutinata* (ca. 5 %) mark the faunal assemblages (Figure 5F-E). The period from ca. 400 – 0 cal yr BP is characterized by a clear increase of *G. bulloides* to ca. 6 %, in addition to a remarkable increase of *G. glutinata* and *G. uvula* (both to ca. 7 %) (Figure 5F; 5E; 5G). *G. uvula* has previously been associated with reduced salinities (e.g. Husum and Hald, 2012) and high food supply related to a productive oceanic front (Saito et al., 1981; Boltovskoy et al., 1996; Bergami et al., 2009).

Both $\delta^{18}O$ and $\delta^{13}C$ show a general depletion within the late Holocene with values in the ranges 3.49 - 3.98 ‰ and 0.34 - 0.84 ‰ for $\delta^{18}O$ and $\delta^{13}C$, respectively (Figure 6). Depleted values of $\delta^{18}O$ most likely reflect warmer temperatures due to an increased influence of Atlantic derived water. The $\delta^{13}C$ record shows a clear depletion towards values below 0.7 ‰, thus indicating enhanced stratification between the surface and sub-surface waters, likely related to a returned influence of Atlantic water.

The late Holocene (ca. 2200 – 0 cal yr BP) is characterized by the highest abundances of $IP_{25}$ (0.35 µg/g OC) and relatively low (but stable) brassicasterol (12.5 µg/g OC) (Figure 7A-B). Although the TOC values fluctuate somewhat throughout the late Holocene, the absolute values (ca. 1.62 %) are the lowest within the entire TOC record (Figure 7C). Consistent with the opposing trends in the $IP_{25}$ and brassicasterol records, the $P_BIP_{25}$ values reach their highest value (0.87) of the record at ca. 0 cal yr BP (Figure 7D). An increase in $P_BIP_{25}$ suggests a further extension in sea ice cover, reflecting Arctic Front conditions (Müller et al., 2011), most similar to modern conditions.

## 5 Holocene palaeoceanographic evolution

Our palaeoceanographic record from the Olga Basin shows generally gradual but distinct changes in seasonal sea ice distribution and Atlantic water inflow to the northern Barents Sea throughout the Holocene. These variations are discussed here, and placed in further context by comparison with previously published records from the region (Figure 1). In terms of sea

ice cover, we interpret our combined proxy data by proposing different seasonal sea ice scenarios. In order to obtain realistic representations for such variations in sea ice cover, we have considered known scenarios derived from modern and historical observations (NSIDC) (Figure 1B). For example, the modern sea ice context has been derived from maximum (March) and seasonal variability (April/August) in sea ice extent using satellite data obtained between 1981 and 2010 (NSIDC) (Figure 8D). In terms of temporal changes, historical data for the Barents Sea show variations in the mean sea ice edge position in April for four sub periods between 1870 and 2002 (i.e. 1870 – 1920; 1921 – 1961; 1962 – 1988; 1989 – 2002) (Divine and Dick, 2006). This north-easterly retreat of the sea ice edge since the second half of the 19$^{th}$ century took place after a significant cooling in the second half of the 18$^{th}$ century and occurred in a north-easterly direction (Divine and Dick, 2006). This key dataset illustrates that, even on a decadal time scale, the migration pattern of the sea ice extent associated with climatic conditions can reflect those observed during seasonal or annual sea ice edge change. Such observations and changes therefore provide precedent for our proposed sea ice scenarios (and changes to these) during the Holocene.

### 5.2 Subpolar conditions and long productive summers ca. 9500 – 5800 cal yr BP

The high relative abundances of *N. pachyderma* in the early part of the record indicate the dominance of Arctic water masses. Nonetheless, the increased abundances of subpolar species and of total planktic foraminifera between ca. 7300 and 5800 cal yr BP indicate a pronounced influence of Atlantic water inflow at the core site, most likely indicative of the HTM. Elevated planktic foraminiferal concentrations were also recorded in the north-eastern Barents Sea around ca. 9800 cal yr BP by Duplessy et al. (2001), who suggested an early intrusion of Atlantic water and high surface water productivity (Figure 1). Similarly, Klitgaard Kristensen et al. (2013) related their observed high planktic foraminiferal concentrations in the northern Barents Sea between ca. 7600 and 6500 cal yr BP to a renewed and stronger influence of Atlantic water (Figure 1). Berben et al. (2014) reached the same conclusion having found a strong increase in the planktic foraminiferal concentrations and relative abundances of subpolar species such as *N. incompta* and *T. quinqueloba* in the western Barents Sea at ca. 10 000 cal yr BP (Figure 1). However, for the West Svalbard margin, Werner et al. (2013) associated high planktic foraminiferal fluxes ca. 8000 cal yr BP to ice-free or seasonally fluctuating sea ice margin conditions (Figure 1).

The depleted stable isotope ($\delta^{18}O$, $\delta^{13}C$) values between ca. 8800 and 7300 cal yr BP most likely reflect the HTM, with the strong enrichment in $\delta^{18}O$ between ca. 7600 and 7300 cal yr BP probably corresponding to the termination phase of the HTM. The latter is consistent with the observations of Duplessy et al. (2001) (Figure 1) who observed decreasing $\delta^{18}O$ values between ca. 10 000 and 7850 cal yr BP and attributed these to a deglacial warming with an increased influence of Atlantic water inflow. Light $\delta^{18}O$ values between ca. 7850 and 6900 cal yr BP were associated with the abrupt termination of the HTM. In addition, Lubinski et al. (2001) linked decreasing $\delta^{18}O$ values between ca. 10 000 and 6800 cal yr BP with a possible surface temperature increase of ca. 1 - 2 °C due to a return inflow of warm water (Figure 1). Klitgaard Kristensen et al. (2013) found low $\delta^{18}O$ values between ca. 7600 and 6500 cal yr BP related to a possible return of stronger inflow of Atlantic water (Figure 1). Similar reports of low $\delta^{18}O$ have be made for a nearby location in the western Barents Sea (ca. 10 000 cal yr BP; Berben et al., 2014) and for the southern Barents Sea (ca. 11 000 – 9500 cal yr BP; Risebrobakken et al., 2010) (Figure 1).

Depleted $\delta^{18}O$ values attributed to a stronger inflow of Atlantic water delivered by the SB have also been recorded at the western and northern Svalbard margin ca. 8000 cal yr BP (Slubowska et al., 2005; Werner et al., 2013) and in the Franz Victoria Trough ca. 7500 cal yr BP (Duplessy et al., 2001) (Figure 1). However, the depleted $\delta^{18}O$ values reported in the current study do not correspond with this observed time-transgressive pattern of the SB and it is assumed, therefore, that throughout the HTM, the core site was influenced by Atlantic water entering the Barents Sea via the NCaC through the BSO. This conclusion is consistent with observations in the southern Barents Sea ca. 11 000 – 9800 cal yr (Risebrobakken et al., 2010) and the north-western Barents Sea ca. 7000 cal yr BP (Klitgaard Kristensen et al., 2013) (Figure 1).

In our record, the increasing $\delta^{13}C$ after ca. 8500 cal yr BP indicates that the early Holocene is further characterized by an increasing trend in primary production and/or less stratified water masses; however, maximum TOC values throughout this period suggest the former, and is consistent with previous findings from the northern Barents Sea (Duplessy et al., 2001; Lubinski et al., 2001), the western Barents Sea (Berben et al., 2014) and the West Svalbard margin (Werner et al., 2013) (Figure 1).

Relatively low $IP_{25}$ concentrations with increased brassicasterol abundances indicate reduced seasonal (spring) sea ice cover and longer (warmer) summers with open water conditions

suitable for phytoplankton production. The occurrence of reduced sea ice cover and longer summers is consistent with increased planktic foraminiferal concentrations (reported here and Carstens et al., 1997) and with longer ice-free seasons and a retreated ice margin in the northern Barents Sea (Duplessy et al., 2001) as well as increased phytoplankton production in the northern Fram Strait (Müller et al., 2009) (Figure 1). Reduced spring sea ice cover also indicates the HTM recorded at the sea surface between ca. 9300 and 6500 cal yr BP, which probably results from maximum summer insolation at 78° N. Similar conclusions regarding the timing and termination of the HTM based on $IP_{25}$ records have been made for the Fram Strait (ending at ca. 8400 cal yr BP; Müller et al., 2009) and at the West Svalbard margin, where the last phase of the HTM was recorded ca. 8500 – 7000 cal yr BP (Müller et al., 2012) (Figure 1).

Previously, Risebrobakken et al. (2011) emphasized that, throughout the HTM, high latitude radiative forcing was not responsible for the overall conditions of the water column and ocean dynamics. They suggested instead, that an intensified heat advection which peaked at ca. 10 000 cal yr BP was the result of a major reorganization of the ocean circulation following the deglaciation. Additionally, atmospheric forcing further enhanced the transport of warm and salty water (Risebrobakken et al., 2011). As the surface layer was directly influenced by the high summer insolation, relatively high air temperatures might also have increased sea surface temperatures which could, additionally, have contributed to reduced seasonal sea ice cover. Further, Smedsrud et al. (2013) showed how increased inflow of Atlantic water via the BSO led to relatively warm and reduced sea ice conditions in the Barents Sea which caused an increased heat flux between the ocean and atmosphere, thus enhancing the formation of dense water. This led to a strong outflow through the BSX, causing a stronger inflow of Atlantic water and thereby maintaining an ocean feedback mechanism. Thus, a strengthening of warm and saline Atlantic water input into the Barents Sea might have contributed to the observed sea ice extent retreat, a possible physical mechanism corresponding to the previously proposed (and recent) 'Atlantification' (Årthun et al., 2012). Consistent with these suggestions, relatively low sea ice biomarker ($IP_{25}$) concentrations are accompanied by maximum brassicasterol abundances which, combined, indicate reduced sea ice cover during relatively short spring seasons, with longer summers leading to enhanced phytoplankton production within the proximity of the sea ice edge. Hence, throughout the early Holocene the sea ice edge was in the proximity of the core site at ca. 78° N (Figure 8A). The elevated brassicasterol concentrations might have resulted from lower seasonality shifts of the sea ice

edge or from longer and warmer summers, so the minimum (summer) sea ice position is less predictable compared to the maximum (Figure 8A). In any case, our proposed sea ice scenario suggests that water masses south of the study area were ice free, which agrees with open water conditions observed in the western Barents Sea (Berben et al., 2014) and the West Svalbard margin (Müller et al., 2012) (Figure 8A) during the early Holocene.

### *5.1.1 Holocene Thermal Maximum: onset and termination*

Within the current study, the proxies indicate the timing of the HTM to be between ca. 9300 and 5800 cal yr BP, although with some differences. The biomarker data record the HTM between ca. 9300 and 6500 cal yr BP, the stable oxygen isotope record indicate maximum temperatures between ca. 8800 and 7300 cal yr BP, whereas the planktic faunal assemblages argue for maximum temperatures from ca. 7300 to 5800 cal yr BP. Since all analyses were carried out on sediment material from the same horizons and the variations in timing (HTM) are larger than the radiocarbon dating errors in the depth-age model (Figure 3), these differences in occurrence and duration of the HTM between proxies demonstrate the variability in proxy-specific response time.

Sea ice biomarkers record the HTM at the sea surface, which is influenced mainly by maximum insolation values. In contrast, the $\delta^{18}O$ record and the faunal assemblages record the HTM within the sub-surface water masses which is the habitat of the polar planktic foraminifera (Volkmann, 2000). These sub-surface water masses are not influenced directly by solar insolation as this is mainly restricted to the sea surface (ca. upper 30 m) (Andersson et al., 2010; Risebrobakken et al., 2011). Hence, the HTM recorded by the oxygen isotopes and planktic foraminiferal fauna reflect warmer water temperatures linked to an increased influence of Atlantic water. A time-transgressive inflow of Atlantic water from south to north along the Norwegian and Svalbard margins as documented by Hald et al. (2007) most likely caused the lag in response time between biomarker and planktic foraminiferal data.

A second lag in response time is observed between the stable isotope and planktic foraminiferal fauna data. The planktic foraminiferal fauna reflect an annual signal whereas, in the Arctic Ocean, the calcification of *N. pachyderma* is linked to phytoplankton blooms and occurs mainly in August (Kohfeld et al., 1996; Volkmann, 2000). However, sea-ice conditions may have caused a shift in the growing season (e.g. Farmer et al., 2008) and it has

also been found that planktic foraminifera may change their depth habitat for the calcification and thus reflect different temperatures compared to the general fauna (Simstich et al., 2003). In particular, *N. pachyderma* is found throughout the upper water column (50 - 100 m), but calcification occurs at depths between 100 - 200 m (e.g. Bauch et al., 1997; Stangeew, 2001; Simstich et al., 2003). Furthermore, the foraminiferal fauna response might also depend on factors other than temperature and salinity. For example, the subpolar species *T. quinqueloba* also depends on the available food supply (e.g. Volkmann, 2000) and increased nutrition might have followed later. Indeed, such a delay in food supply is suggested by increasing $\delta^{13}C$ values which likely reflect enhanced primary production, possibly associated with increased seasonal sea ice cover. After ca. 6500 cal yr BP, the increased concentrations of sea ice biomarkers certainly argue for the appearance of a MIZ which is associated with a high food supply on which *T. quinqueloba* seems to thrive (e.g. Volkmann, 2000). Hence, the timing of increased relative abundances of subpolar species is probably related to a combination of enhanced Atlantic water influence and increased nutrition availability due to a strengthening of the seasonal sea ice cover. Such a conclusion agrees with the observation of the HTM associated with Atlantic water, high primary productivity and food availability in the northern Barents Sea (Duplessy et al., 2001).

### 5.2 Well-ventilated water masses and moderated seasonality ca. 5800 – 2200 cal yr BP

Throughout the mid Holocene, the relative abundances of the subpolar foraminifera decrease indicating a reduced influence of Atlantic water inflow. In addition, the clear and stable dominance of *N. pachyderma* demonstrate the prevailing presence of Arctic water at the core site. Correspondingly, the enriched $\delta^{18}O$ values argue for lower temperatures consistent with previous records. Most notably, a similar cooler mid Holocene with a strongly reduced Atlantic water inflow and/or colder Atlantic water has been observed in the northern Barents Sea (Duplessy et al., 2001; Klitgaard Kristensen et al., 2013) (Figure 1) and it has also been suggested that Arctic water from the north-eastern Barents Sea might have influenced the western Barents Sea due to less heat advection from the south (Hald et al., 2007). In the eastern Fram Strait, Werner et al. (2013) observed cold conditions after ca. 5200 cal yr BP, with a profound decrease of *T. quinqueloba* and low planktic foraminiferal fluxes (Figure 1).

Compared with the early Holocene, lower TOC values indicate that the enriched $\delta^{13}C$ values reflect better ventilation of the water masses throughout the mid Holocene, consistent with previous research (Spielhagen and Erlenkeuser, 1994). For the northern Barents Sea, Lubinski et al. (2001) suggested that enriched $\delta^{13}C$ values might even reflect the ventilation conditions over a broad area (Figure 1) and similar $\delta^{13}C$ trends have indeed been reported for the northern Barents Sea (Duplessy et al., 2001), the western Barents Sea (Berben et al., 2014) and the West Svalbard margin (Werner et al., 2013) (Figure 1).

For the biomarkers, higher concentrations of $IP_{25}$ with concomitant decreases in brassicasterol indicate an increased and consistent seasonal sea ice cover and similar $IP_{25}$-based observations of sea ice have been linked to the mid Holocene Neoglacial cooling for the northern Fram Strait (Müller et al., 2009) and West Svalbard margin (Müller et al., 2012) (Figure 1).

Overall, the climatic changes show a period marked by a continuous cooling trend with a dominance of cold Arctic water and an accompanying increase in seasonal sea ice cover. As the summer insolation decreased, it probably caused the surface layer to cool with increased production of seasonal sea ice. Consequently, the strongly reduced Atlantic water inflow could not have affected the sea ice distribution in the same way as was proposed for the early Holocene (i.e. via the ocean feedback mechanism). These changes are translated into a scenario consisting of an overall advance of the sea ice extent (Figure 8B). The minimum sea ice edge was probably further south compared to the early Holocene, consistent with previous observations in the northern Barents Sea after ca. 6000 cal yr BP. For example, Duplessy et al. (2001) recorded a southwards shift of the summer sea ice margin and Klitgaard Kristensen et al. (2013) argued for generally increased sea ice cover, with the MIZ advancing towards the south (Figure 8B). In the northern Fram Strait, Müller et al. (2009) found very low (almost absent) amounts of brassicasterol and increased concentrations of $IP_{25}$, which also indicates a more general southwards advance of the minimum sea ice edge at this time (Figure 8B). During winter, we suggest that the maximum sea ice edge ranged between 76 - 77° N or, at least, further south compared to the early Holocene (Figure 8A-B) and corresponds well to the sea ice conditions inferred from $IP_{25}$ measurements at the continental slope of western Svalbard (Müller et al., 2012) (Figure 8B). In the western Barents Sea, however, $IP_{25}$ was mainly absent, reflecting predominantly ice free conditions during this interval (Berben et al., 2014) (Figure 8B).

### 5.3 Stratified water masses and long icy winters ca. 2200 – 0 cal yr BP

The general decrease of *N. pachyderma* and increased relative abundances of subpolar foraminifera, indicate a returned influence of Atlantic water during the late Holocene. In addition to the overall observed trend, the planktic foraminiferal concentrations and fauna show additional fluctuations that argue for intervals of varying Atlantic water influence, an observation supported by an overall depleting trend and periods of even more depleted $\delta^{18}O$ values. These observations agree well with previous reports of more unstable oceanographic conditions throughout the late Holocene with episodic increases in Atlantic water into the northern Barents Sea (Duplessy et al., 2001; Lubinski et al., 2001), the western Barents Sea (Wilson et al., 2011; Berben et al., 2014) and the Svalbard margin (Jernas et al., 2013; Werner et al., 2013) (Figure 1).

An overall depletion in $\delta^{13}C$ values indicates enhanced stratification between the surface and sub-surface layers. A similar trend was found within the northern Barents Sea after ca. 3000 cal yr BP and was attributed to decreased ventilation and/or decreased primary production (Duplessy et al., 2001; Lubinski et al., 2001; Risebrobakken et al., 2011) (Figure 1). In addition, Werner et al. (2013) suggested that gradually decreasing $\delta^{13}C$ values at the West Svalbard margin could also be related to the density-driven downward migration of *N. pachyderma* as a response to the less-ventilated sub-surface waters (Kozdon et al., 2009) (Figure 1). The latter is suggested to be a result of the thickening of the surface layer due to the influence of sea ice and a freshening of the uppermost surface water layer. Werner et al. (2013) also found a similar increased in *G. uvula* throughout the late Holocene and noted similar findings at the south-west Svalbard margin (Rasmussen et al., 2007) (Figure 1) which were attributed to an increased contribution of cool productive coastal waters according to Husum and Hald (2012). A similar increased relative abundance of *G. uvula* was found in the western Barents Sea throughout the last ca. 1100 cal yr BP (Berben et al., 2014), and this was associated with slightly reduced salinities (Figure 1). However, since *G. uvula* is a rather small species, the increased relative abundance could also be created by the advection of tests by Atlantic water transport.

An increase in sea ice during the late Holocene is also indicated from the biomarker ($IP_{25}$) data. Previously, Berben et al. (2014) reported increased $IP_{25}$ concentrations throughout the last ca. 1100 cal yr BP in the western Barents Sea, arguing for a south-westwards transgression of the sea ice edge (Figure 1). Further, and consistent with the episodes of

elevated planktic foraminiferal concentrations, the biomarker and TOC data also reveal episodes where the general trend is amplified (i.e. simultaneous increase in sea ice and phytoplankton biomarkers), most likely indicating intervals of intensified primary production. An intensified sea ice cover with intervals of sea ice fluctuations was also observed in the eastern Fram Strait throughout the last 3000 cal yr BP (Müller et al., 2012) (Figure 1).

Compared to the early Holocene, the observed sub-surface warming versus a sea surface cooling might seem contradictory, but indicates that the late Holocene was most likely characterized by a strong vertical stratification and a decoupling between the atmosphere and the oceanic sub-surface. Summer insolation was lower during the late Holocene resulting in cooler atmospheric temperatures and potentially enhanced sea ice production and/or reduced sea ice melt. In addition to the stronger vertical stratification of the water column, the increased sea ice cover probably also limited the heat flux between the atmosphere and the sub-surface water masses. In terms of seasonality, we suggest that relatively long spring seasons with extensive sea ice cover and maximum $IP_{25}$ would have been followed by shorter (and probably cooler compared to previous periods) summers with lower phytoplankton production (brassicasterol) (Figure 8C). Overall, the site was characterized by an extensive sea ice cover with the maximum (and possibly minimum) sea ice edge further south of the core site (Figure 8C). Our observations and interpretations are also consistent with intensified sea ice occurrence in the northern Barents Sea (Duplessy et al., 2001; Klitgaard Kristensen et al., 2013), increasing sea ice cover in the Fram Strait (Müller et al., 2009; 2012) and the western Barents Sea (Berben et al., 2014) (Figure 8C). Finally, we note that concentrations of $IP_{25}$ and brassicasterol in surface sediment material from a nearby location (78.39° N, 32.07° E; Navarro-Rodriguez, 2014) are, respectively, slightly lower and higher than those in the upper sections of the NP05-11-70GC core. We interpret these data as representing a slight reversal in the extent of spring sea ice cover during recent decades (Figure 8D) and a return to more open water conditions during summer (c.f. Mid Holocene). Of course, precedent for such a reversal in sea ice extent is evident during the last ca. 100 yr from observational records (Divine and Dick, 2006), but the biomarker data provide further evidence that sea ice cover likely exceeded the modern extent during the (pre-industrial) late Holocene (Figure 8C).

### *5.2.1 Sub-surface warming versus increased sea ice extent*

The observed increase in sea ice extent corresponds well with the overall cooling throughout the late Holocene as recorded previously by various Arctic terrestrial (e.g. Bjune et al., 2009; Kaufman et al., 2009), ice core (e.g. Kaufman et al., 2009; Divine et al., 2011) and marine records (e.g. Slubowska et al., 2005; Skirbekk et al., 2010). The overall increased sea ice extent is most likely a direct result of the low insolation directly affecting the sea surface, possibly strengthened by a negative solar irradiance anomaly between ca. 2850 and 2600 cal yr BP which would have triggered the increased sea ice extent and decreased ventilation of the sub-surface waters. The probability of such a mechanism was illustrated further by a modelling experiment performed by Renssen et al. (2006).

The increased influence of Atlantic water inflow also correlates well to previous studies arguing for warmer sub-surface water masses throughout the late Holocene in the Barents Sea (Lubinski et al., 2001; Duplessy et al., 2005; Risebrobakken et al., 2010; Wilson et al., 2011) and at the Svalbard margin (Jernas et al., 2013; Werner et al., 2013). The increased Atlantic water influence is attributed to prevailing positive North Atlantic Oscillation (NAO) conditions, amplified by stronger stratification among the upper layers (Lubinski et al., 2001; Duplessy et al., 2005).

As it is suggested here that a positive NAO situation could have forced the general increased influence of Atlantic water, it might be that even more pronounced positive NAO conditions caused the observed intervals showing amplified conditions of Atlantic water inflow. Thus, Duplessy et al. (2005) correlated their minor fluctuations in temperatures to centennial to millennial-scale variations in the intensity of westerlies in the North Atlantic. These intervals also show further elevated levels of sea ice and phytoplankton biomarker concentrations. Müller et al. (2012) observed similar in-phase fluctuations of $IP_{25}$ and phytoplankton biomarkers in the eastern Fram Strait and assumed that they might have been triggered by a temporarily strengthened inflow of Atlantic water and/or changed atmospheric circulation pattern and also argue that positive NAO-like conditions could have prevailed during intervals of elevated biomarker contents.

## 6 Conclusions

Holocene palaeoceanographic evolution in the northern Barents Sea has been reconstructed using multi-proxy data obtained from a marine sediment core taken from the Olga Basin. The observed changes of Atlantic water inflow and seasonal sea ice cover have illustrated natural oceanic variability and some possible physical driving forces and aspects of ocean-sea ice-atmosphere dynamics are discussed. Three major palaeoceanographic settings can be summarised as follows:

*The early Holocene (ca. 9500 – 5800 cal yr BP)*

Overall warm subpolar conditions, i.e. a pronounced inflow of Atlantic water, a reduced seasonal sea ice cover and an increased primary production, were determined, primarily, by the high summer insolation. The core site was influenced by Atlantic water entering the Barents Sea via the NCaC through the BSO which caused an increased heat flux between the ocean and the atmosphere. This led to an active ocean feedback mechanism that contributed to a reduced sea ice extent. Seasonally, the interval was characterised by short spring seasons, long productive summers and potentially less variability in sea ice. Some differences in the timing of the HTM between ca. 9300 and 5800 cal yr BP are attributed to proxy-specific responses. We suggest that sea ice responded most directly to solar insolation at the sea surface, whereas sub-surface water masses were more influenced by the inflow of Atlantic water. Stable isotopes (foraminifera) responded to changes in temperature and salinity changes, whereas the planktic foraminiferal distributions also depended on food availability. Furthermore, the latter two proxies reflect different seasons throughout the year and/or different depth habitats.

*The mid Holocene (ca. 5800 – 2200 cal yr BP)*

In this interval, an overall cooling trend was characterized by cold Arctic water, well-ventilated water masses and an advanced seasonal sea ice cover. These are associated with the Neoglacial cooling, consistent with reduced summer insolation at high latitudes. Due to the lowered summer insolation, reduced atmospheric temperatures likely affected sea surface conditions and increased sea ice production. This interval was also characterized by a general increase southwards in sea ice edge position during winter and summer.

*The late Holocene (ca. 2200 – 0 cal yr BP)*

This period was marked by an increased Atlantic water inflow, enhanced stratification and extensive seasonal sea ice cover. The overall increased sea ice cover was probably induced by lowered insolation. The observed sub-surface warming and sea surface cooling co-existed due to a decoupling between the atmosphere and the ocean, with the sea ice acting as a barrier between the two. Long spring seasons with extensive sea ice cover were followed by relatively short and less productive summers. Sea ice distribution was at its greatest extent within the entire record. Some reversal of sea ice expansion is proposed in recent decades. Elevated levels of Atlantic water inflow, primary production and seasonal sea ice cover suggest more unstable oceanographic conditions. These intervals are attributed to more pronounced positive NAO-like conditions that amplified the general trends.

## Acknowledgements

This work was carried out within the framework of the Initial Training Network program "Changing Arctic and Subarctic Environments" (CASE, Grant Agreement No. 238111) funded by the European Commission within the 7th Framework Program People, the Research Council of Norway in addition to the University of Tromsø and Norwegian Polar Institute. Thanks are also extended to Trine Dahl and Julia Sen for assisting with laboratory work in addition to Patricia Cabedo-Sanz for valuable discussions.

# References


Aagaard K and Greisman P (1975) Towards new mass and heat budgets in the Arctic Ocean. *J. Geophys. Res.* 80: 3821-3827.

Abrahamsen E, Østerhus S and Gammelsrød T (2006) Ice draft and current measurements from the north-western Barents Sea, 1993-96. *Polar Res.* 25: 25-37.

Aksenov Y, Bacon S, Coward AC and Nurser AJG (2010) The North Atlantic inflow to the Arctic Ocean: high-resolution model study. *J. Mar. Syst.* 79: 1-22.

Aksu AE and Vilks G (1988) Stable isotopes in planktonic and benthic foraminifera from Arctic Ocean surface sediments. *Can. J. Earth Sci.* 25: 701-709.

Andersson C, Pausata FSR, Jansen E, Risebrobakken B and Telford RJ (2010) Holocene trends in the foraminifer record from the Norwegian Sea and the North Atlantic Ocean. *Clim. Past* 6: 179-193, doi:10.5194/cp-6-179-2010.

Årthun M, Ingvaldsen RB, Smedsrud LH and Schrum C (2011) Dense water formation and circulation in the Barents Sea. *Deep-Sea Res. I* 58: 801-817.

Årthun M, Eldevik T, Smedsrud LH, Skagseth Ø and Ingvaldsen R (2012) Quantifying the influence of Atlantic heat on Barents Sea ice variability and retreat. *J. Clim.* 25: 4736-4743.

Barker S and Elderfield H (2002) Foraminiferal calcification response to glacial interglacial changes in atmospheric $CO_2$. *Science* 297: 883-836.

Barker S, Kiefer T and Elderfield H (2004) Temporal changes in North Atlantic circulation constrained by planktonic foraminiferal shell weights. *Paleoceanography* 19: PA3008.

Bauch D, Carstens J and Wefer G (1997) Oxygen isotope composition of living Neogloboquadrina pachyderma (sin.) in the Arctic Ocean. *Earth Planet. Sc. Lett.* 146: 47-58.

Bauch D, Carstens J, Wefer G and Thiede J (2000) The imprint of anthropogenic $CO_2$ in the Arctic Ocean: evidence from planktic $d^{13}C$ data from water column and sediment surfaces. *Deep-Sea Res. Pt. II* 9-11: 1791-1808.

Bé AWH and Tolderlund DS (1971) Distribution and ecology of living planktonic foraminifera in surface waters of the Atlantic and Indian Oceans. In Funnell BM and Riedel WR (eds) *The micropaleontology of oceans.* Cambridge University Press, London, 105-149.

Beer CJ, Schiebel R and Wilson PA (2010) Testing planktic foraminiferal shell weight as a surface water [$CO_3^{2-}$] proxy using plankton net samples. *Geology* 38: 103-106.

Belt ST, and Müller J (2013) The Arctic sea ice biomarker $IP_{25}$: a review of current understanding, recommendations for future research and applications in palaeo sea ice reconstructions. *Quaternary Sci. Rev. Doi: 10.1016/j.quascirev.2012.12.001.*

Belt ST, Massé G, Rowland SJ, Poulin M, Michel C and LeBlanc B (2007) A novel chemical fossil of palaeo sea ice: $IP_{25}$. *Org. Geochem.* 38: 16-27.

Belt ST, Brown TA, Navarro Rodriguez A, Cabedo Sanz P, Tonkin A and Ingle R (2012) A reproducible method for the extraction, identification and quantification of the Arctic sea ice proxy $IP_{25}$ from marine sediments. *Anal. Method.* 4: 705-713.

Berben SMP, Husum K, Cabedo-Sanz P and Belt ST (2014) Holocene sub-centennial evolution of Atlantic water inflow and sea ice distribution in the western Barents Sea. *Clim. Past* 10: 181-198, doi:10.5194/cp-10-181-2014.

Bergami C, Capotondi L, Langone L, Giglio F and Ravaioli M (2009) Distribution of living planktonic foraminifera in the Ross Sea and the Pacific sector of the Southern Ocean (Antarctica). *Mar. Micropaleontol*. 73: 37-48.

Berger A (1978) Long-term variations of daily insolation and quaternary climatic changes. *J. Atmos. Sci.* 35: 2363-2367.

Bjune AE, Seppä H and Birks HJB (2009) Quantitative summer temperature reconstructions for the last 2000 years based on pollen-stratigraphical data from northern Fennoscandia. *J. Paleolimnol.* 41: 43-56.

Boltovskoy E, Boltovskoy D, Correa N and Brandini F (1996) Planktic foraminifera from the southwestern Atlantic (30° – 60°S): Species-specific patterns in the upper 50 m. *Mar. Micropaleontol.* 28: 53–72.

Broecker WS and Clark E (2001) An evaluation of Lohmann's foraminifera weight dissolution index. *Paleoceanography* 16: 531-534.

Brown TA and Belt ST (2012) Identification of the sea ice diatom biomarker $IP_{25}$ in Arctic benthic macrofauna: Direct evidence for a sea ice diatom diet in Arctic heterotrophs. *Polar Biol.* 35: 131-137.

Brown TA, Belt ST, Philippe B, Mundy CJ, Massé G, Poulin M and Gosselin M (2011) Temporal and vertical variations of lipid biomarkers during a bottom ice diatom bloom in the Canadian Beaufort Sea: Further evidence for the use of the $IP_{25}$ biomarker as a proxy for spring Arctic sea ice. *Polar Biol.* 34: 1857-1868.

Brown TA, Belt ST, Tatarek A and Mundy CJ (2014) Source identification of the Arctic sea ice proxy $IP_{25}$. *Nat. Commun.* 5:4197 doi: 10.1038/ncomms5197.

Burhol ALS (1994) Recent distribution of planktonic foraminifera on the Svalbard-Barents margin. Master Thesis, University of Tromsø, Tromsø, Norway.

Carmack E, Barber D, Christensen J, Macdonald R, Rudels B and Sakshaug E (2006) Climate variability and physical forcing of the food webs and the carbon budget on panarctic shelves. *Prog. Oceanogr.* 71: 145-181.

Carstens J, Hebbeln D and Wefer G (1997) Distribution of planktic foraminifera at the ice margin in the Arctic (Fram Strait). *Mar. Micropaleontol.* 29: 257-269.

Cifelli R (1961) Globigerina incompta, a new species of pelagic foraminifera from the North Atlantic. *Contributions Cushman Foundation Foraminiferal Research* 12: 83-86.

Conan SMH, Ivanova EM and Brummer G-JA (2002) Quantifying carbonate dissolution and calibration of foraminiferal dissolution indices in the Somali Basin. *Mar. Geol.* 182: 325-349.

Dahl-Jensen D, Moesgaard K, Gundestrup N, Clow GD, Johnsen SJ, Hansen AW and Balling N (1998) Past temperatures directly from the Greenland Ice Sheet. *Science* 282: 268-271.

Darling KF, Kucera M, Kroon D and Wade CM (2006) A resolution for the coiling direction paradox in Neogloboquadrina pachyderma. *Paleoceanography* 21: PA2011, doi:10-1029/2005PA001189.

Divine DV and Dick C (2006) Historical variability of sea ice edge position in the Nordic Seas. *J. Geophys. Res.* 111: C01001, doi:10.1029/2004JC002851.

Divine D, Isaksson E, Martma T, Meijer HAJ, Moore J, Pohjola V, van de Wal RSW and Godtliebsen F (2011) Thousand years of winter surface air temperature variations in Svalbard and northern Norway reconstructed from ice-core data. *Polar Research* 30: 7379, doi: 10.3402/polar.v30i0.7379.

Donner B and Wefer G (1994) Flux and stable isotope composition of Neogloboquadrina pachyderma and other planktonic foraminifers in the Southern Ocean (Atlantic sector). *Deep-Sea Res. Pt. I* 41: 1733-1743.

Duplessy JC, Ivanova E, Murdmaa I, Paterne M and Labeyrie L (2001) Holocene paleoceanography of the northern Barents Sea and variations of the northward heat transport by the Atlantic Ocean. *Boreas* 30: 2-16.

Duplessy JC, Cortijo E, Ivanova E, Khusid T, Labeyrie L, Levitan M, Murdmaa I and Paterne M (2005) Paleoceanography of the Barents Sea during the Holocene. *Paleoceanography* 20: A4004.

Ehrmann WU and Thiede J (1985) History of Mesozoic and Cenozoic sediment fluxes to the North Atlantic Ocean. Contributions to Sedimentology E. Schweizerbart'sche Verlagsbuchhandlung, Stuttgart, 15: 1-109, ISBN 3-510-57015-4.

Ellingsen I, Slagstad D and Sundfjord A (2009) Modification of water masses in the Barents Sea and its coupling to ice dynamics: A model study. *Ocean. Dyn.* 59: 1095-1108.

Fairbanks RG (1989) A 17 000-year glacia-eustatic sea level record: Influence of glacial melting rates on the Younger Dryas event and deep-ocean circulation. *Nature* 342: 637-642.

Farmer EJ, Chapman MR and Andrews JE (2008) Centennial-scale Holocene North Atlantic surface temperatures from Mg/Ca ratios in *Globigerina bulloides*, *Geochemistry, Geophysics, Geosystems*. Epub ahead of print 31December, DOI: 10.1029/2008GC002199.

Forcino FL (2012) Multivariate assessment of the required sample size for community paleoecological research. *Palaeogeogr. Palaeocl.* 315-316: 134-141.

Gammelsrød T, Leikvin Ø, Lien V, Budgell WP, Loeng H and Maslowski W (2009) Mass and heat transports in the NE Barents Sea: Observations and models. *J. Marine Syst.* 75: 56-69.

Hald M, Andersson C, Ebbesen H, Jansen E, Klitegaard-Kristensen D, Risebrobakken B, Salomonsen GR, Sejrup HP, Sarnthein M and Telford R (2007) Variations in temperature and extent of Atlantic water in the northern North Atlantic during the Holocene. *Quaternary Sci. Rev.* 26: 3423-3440.

Hebbeln D, Henrich R and Baumann K-H (1998) Paleoceanography of the last glacial/interglacial cycle in the Polar North Atlantic. *Quat. Sci. Rev.* 17: 125-153.

Henrich R, Baumann KH, Huber R and Meggers H (2002) Carbonate preservation records of the past 3Myr in the Norwegian-Greenland Sea and the northern North Atlantic: Implications for the history of NADW production. *Mar. Geol.* 184: 17-39.

Hopkins TS (1991) The GIN Sea: A synthesis of its physical oceanography and literature review, 1972–1985. *Earth Sci. Rev.* 30: 175-318.

Huber R, Meggers H, Baumann KH and Henrich R (2000) Recent and Pleistocene carbonate dissolution in sediments of the Norwegian-Greenland Sea. *Mar. Geol.* 165: 123-136.

Husum K and Hald M (2004) A continuous marine record 8000–1600 cal. yr BP from the Malangenfjord, north Norway: Foraminiferal and isotopic evidence. *Holocene* 14: 877-887.

Husum K and Hald M (2012) Arctic planktic foraminiferal assemblages: Implications for subsurface temperature reconstructions. *Mar. Micropaleontol.* 96-97: 38-47.

Jakobsson M, Grantz A, Kristoffersen Y and Macnab R (2004) Physiography and bathymetry of the Arctic Ocean. In: Stein R and Macdonald RW (eds) *The Organic Carbon Cycle in the Arctic Ocean*. Springer, New York, 1-5.

Jernas P, Klitgaard Kristensen D, Husum K, Wilson L and Koç N (2013) Palaeoenvironmental changes of the last two millennia on the western and northern Svalbard shelf. *Boreas* 42: 236-255.

Johannessen T, Jansen E, Flatøy A and Ravelo AC (1994) The relationship between surface water masses, oceanographic fronts and plaeoclimatic proxies in surface sediments of the Greenland, Iceland, Norwegian Seas. In: Zahn R, Pedersen TF, Kaminski MA and Labeyrie L (eds) *Carbon Cycling in the Glacial Ocean: Constraints of the Ocean's Role in Global Change*. Springer, Berlin, 61-86.

Jonkers L, Brummer G-JA, Peeters FJC, van Aken HM and De Jong MF (2010) Seasonal stratification, shell flux, and oxygen isotope dynamics of left-coiling N. pachyderma and T. quinqueloba in the western sub polar North Atlantic. *Paleoceanography* 25: PA2204.

Kaufman D, Ager TA, Anderson NJ, Anderson PM, Andrews JT, Bartlein PJ, Brubakker LB, Coats LL, Cwynar LC, Duvall ML, Dyke AS, Edwards ME, Eisner WR, Gajewski K, Geirsdottir A, Hu FS, Jennings AE, Kaplan MR, Kerwin MW, Loshkin AV, MacDonald GM, Miller GH, Mock CJ, Oswald WW, Otto-Bliesner BL, Porinchu DF, Rühland K, Smol JP, Steig EJ and Wolfe BB (2004) Holocene thermal maximum in the western Arctic (0 - 180 °N). *Quaternary Sci. Rev.* 23: 529-560.

Kaufman DS, Schneider DP, McKay NP, Ammann CM, Bradley RS, Briffa KR, Miller GH, Otto-Bliesner BL, Overpeck JT and Vinther BM (2009) Recent warming reverses long-term arctic cooling. *Science* 325(5945): 1236-1239.

Keigwin LD and Boyle EA (1989) Late Quaternary paleochemistry of high-latitude surface waters. *Palaeogeogr. Palaeocl.* 73: 85-106.

Klitgaard Kristensen D, Rasmussen TL and Koç N (2013) Paleoceanographic changes in the northern Barents Sea during the last 16 000 years – new constraints on the last deglaciation of the Svalbard-Barents Ice Sheet. *Boreas* 42: 798-813.

Knudsen KL (1998) Foraminiferer i Kvartær stratigrafi: Laboratorie og fremstillingsteknik samt udvalgte eksempler. *Geologisk Tidsskrift* 3: 1-25.

Koç N, Jansen E and Haflidason H (1993) Paleoceanographic reconstructions of surface ocean conditions in the Greenland, Iceland and Norwegian seas through the last 14 ka based on diatoms. *Quaternary Sci. Rev.* 12: 115-140.

Kohfeld KE, Fairbanks RG and Smith SL (1996) *Neogloboquadrina pachyderma* (sinistral coiling) as paleoceanographic tracers in polar oceans: Evidence from northeast water polynya plankton tows, sediments traps, and surface sediments. *Paleoceanography* 11: 679-699.

Kozdon R, Eisenhauer A, Weinelt M, Meland MY and Nuernberg D (2009) Reassessing Mg/Ca temperature calibrations of Neogloboquadrina pachyderma (sinistral) using paired d44/40Ca and Mg/Ca measurements. *Geochem. Geophys. Geosyst.* 10: Q03005, doi:10.1029/2008GC002169.

Kwok R (2009) Outflow of Arctic Ocean sea ice into the Greenland and Barents Seas: 1979-2007. *J. Clim.* 22(9): 2438-2457.

Kwok R, Maslowski W and Laxon S (2005) On large outflows of Arctic sea-ice into the Barents Sea. *Geophys. Res. Lett.* 32: L22503. Doi:10.1029/2005GL024485.

Laskar J, Robutel P, Joutel F, Gastineau M, Correia ACM and Levrard B (2004) A long-term numerical solution for the insolation quantities of the Earth. *Astron. Astrophys.* 428: 261-285.

Loeng H (1991) Features of the physical oceanographic conditions of the Barents Sea. *Polar Res.* 10: 5-18.

Loeng H, Ozhigin V, Ådlandsvik B and Sagen H (1993) Current Measurements in the northeastern Barents Sea. International Council for the Exploration of the Sea, Council Meeting 1993/C:41, Hydrographic Committee, 22.

Lubinski DJ, Polyak L and Forman SL (2001) Freshwater and Atlantic water inflows to the deep northern Barents and Kara seas since ca 13 $^{14}$Cka: foraminifera and stable isotopes. *Quaternary Sci. Rev.* 20: 1851-1879.

Mangerud J, Bondevik S, Gulliksen S, Hufthammer AK and Høisæter T (2006) Marine $^{14}$C reservoir ages for 19$^{th}$ century whales and molluscs from the North Atlantic. *Quaternary Sci. Rev.* 25: 3228-3245.

Manley TO (1995) Branching of Atlantic water within the Greenland—Spitsbergen passage: an estimate of recirculation. *J. Geophys. Res.* 100: 20627-20634.

Midttun L (1985) Formation of dense bottom water in the Barents Sea *Deep-Sea Res.* 32: 1233-1241.

Moros M, Emeis K, Risebrobakken B, Snowball I, Kuijpers A, McManus J and Jansen E (2004) Sea surface temperatures and ice rafting in the Holocene North Atlantic: Climate influences on northern Europe and Greenland. *Quaternary Sci. Rev.* 23: 2113-2126.

Müller J, Massé G, Stein R and Belt ST (2009) Variability of sea-ice conditions in the Fram Strait over the past 30000 years. *Nat. Geosci.* 2 (11): 772-776.

Müller J, Wagner A, Fahl K, Stein R, Prange M and Lohman G (2011) Towards quantitative sea ice reconstructions in the northern North Atlantic: A combined biomarker and numerical modelling approach. *Earth Planet. Sci. Lett.* 306: 137-148.

Müller J, Werner K, Stein R, Fahl K, Moros M and Jansen E (2012) Holocene cooling culminates in sea ice oscillations in Fram Strait. *Quaternary Sci. Rev.* 47: 1-14.

National Snow and Ice Data Center (NSIDC), Boulder Colorado, www.nsidc.com

Navarro-Rodriguez A (2014) Reconstruction of recent and palaeo sea ice conditions in the Barents Sea. PhD Thesis, Plymouth University, Plymouth, UK.

Novitskiy VP (1961) Permanent currents of the northern Barents Sea. *Tr. Gos. Okeanogr. Inst.* 64: 1-32. (English Translation)

Oppo DW and Fairbanks RG (1989) Carbon isotope composition of tropical surface water during the past 22,000 years. *Paleoceanography* 4: 333-351.

Pfirman SL, Bauch D and Gammelsrød T (1994) The Northern Barents Sea: water mass distribution and modification. In: Johannessen OM, Muench RD and Overland JE (eds) *The Polar Oceans and Their Role in Shaping the Global Environment*. *AGU Geoph. Monog. Series.* 85: 77-94.

Pfuhl HA and Shackleton NJ (2004) Two proximal, high-resolution records of foraminiferal fragmentation and their implications for changes in dissolution. *Deep-Sea Res. Pt. I* 51: 809-832.

Rasmussen TL, Thomsen E, Slubowska MA, Jessen S, Solheim A and Koç N (2007) Paleoceanographic evolution of the SW Svalbard margin (76 °N) since 20 000 $^{14}$C yr BP. *Quaternary Res.* 67: 100-114.

Rasmussen TL, Forwick M and Mackensen A (2012) Reconstruction of inflow of Atlantic Water to Isfjorden, Svalbard during the Holocene: Correlation to climate and seasonality. *Mar. Micropaleontol.* 94-95: 80-90.

Reimer PJ, Baillie MGL, Bard E, Bayliss A, Beck JW, Blackwell PG, Ramsey CB, Buck CE, Burr GS, Edwards RL, Friedrich HM, Grootes PM, Guilderson TP, Hajdas I, Heaton TJ, Hogg AG, Hughen KA, Kaiser KF, Kromer B, Mccormac FG, Manning SW, Reimer RW, Richards DA, Southon JR, Talamo S, Turney CSM, Van Der Plicht J and Weyhenmeyer CE (2009) IntCal09 and Marine09 radiocarbon age calibration curves, 0-50 000 years cal BP. *Radiocarbon* 51: 1111-1150.

Renssen H, Goosse H and Muscheler R (2006) Coupled climate model simulation of Holocene cooling events: oceanic feedback amplifies solar forcing. *Clim. Past* 2: 79-90, doi:10.5194/cp-2-79-2006.

Reynolds L and Thunnel RC (1985) Seasonal succession of planktonic foraminifera in the subpolar North Pacific. *J. Foramin. Res.* 15: 282-301.

Risebrobakken B, Morros M, Ivanova EV, Chistyakova N and Rosenberg R (2010) Climate and oceanographic variability in the SW Barents Sea during the Holocene. *Holocene* 20: 609-621.

Risebrobakken B, Dokken T, Smedsrud LH, Andersson C, Jansen E, Moros M and Ivanova EV (2011) Early Holocene temperature variability in the Nordic Seas: The role of oceanic heat advection versus changes in orbital forcing. *Paleoceanography* 26: PA4206.

Rudels B (1987) On the mass balance of the Polar Ocean, with special emphasis on the Fram Strait. *Norsk Polarinst. Skri.* 188: 53.

Saito T, Thompson PR and Breger D (1981) Systematic index of recent and pleistocene planktonic foraminifera. University of Tokyo press, Tokyo, Japan.

Sakshaug E, Bjørge A, Gulliksen B, Loeng H and Mehlum F (1992) Økosystem Barentshavet. Norges Allmenvitenskapelige Forskningsråd, Norges Fiskeriforskningsråd, Miljøverndepartementet, 304.

Sarnthein M, Van Kreveld S, Erlenkeuser H, Grootes PM, Kucera M, Pflaumann U and Schulz M (2003) Centennial- to millennial-scale periodicities of Holocene climate and sediment injections off the western Barents shelf, 75 N. *Boreas* 32: 447-461.

Schauer U, Loeng H, Rudels B, Ozhigin VK and Dieck W (2002) Atlantic Water flow through the Barents and Kara Seas. *Deep-Sea Res. I* 49: 2281-2298.

Scott DB, Schell T, Rochon A and Blasco S (2008) Modern benthic foraminifera in the surface sediments of the Beaufort shelf, slope and Mackenzie Through, Beaufort Sea, Canada: Taxonomy and summary of surficial distributions. *J. Foramin. Res.* 38: 228-250.

Screen JA and Simmonds I (2010) The central role of diminishing sea ice in recent Arctic temperature amplification. *Nature* 464: 1334-1337.

Serreze M, Barrett A, Slater A, Steele M, Zhang J and Trenberth K (2007) The large-scale energy budget of the Arctic. *J. Geophys. Res.* 112: D11122, doi.:10.1029/2006JD008230.

Simstich J, Sarnthein M and Erlenkeuser H (2003) Paired $\delta^{18}O$ signals of N. pachyderma (s) and T. quinqueloba show thermal stratification structure in the Nordic Seas *Mar. Micropaleontol.* 48: 107-125.

Skirbekk K, Klitgaard Kristensen D, Rasmussen TL, Koç N and Forwick M (2010) Holocene climate variations at the entrance to a warm Arctic fjord: evidence from Kongsfjorden trough, Svalbard. *Geological society, London, Special Publications 2010* 344: 289-304, doi:10.1144/SP344.20.

Slubowska MA, Koç N, Rasmussen TL and Klitgaard-Kristensen D (2005) Changes in the flow of Atlantic water into the Arctic Ocean since the last deglaciation: Evidence from the northern Svalbard continental margin, 80N. *Paleoceonography* 20: PA4014, doi:10.1029/2005PA001141.

Slubowska-Woldengen M, Rasmussen TL, Koç N, Klitgaard-Kristensen D, Nilsen F and Solheim A (2007) Advection of Atlantic Water to the western and northern Svalbard shelf since 17 500 cal yr BP. *Quaternary Sci. Rev.* 26: 463-478.

Smedsrud LH, Esau I, Ingvaldsen RB, Eldevik T, Haugan PM, Li C, Lien VS, Olsen A, Omar AM, Otterå OH, Risebrobakken B, Sandø AB, Semenov VA and Sorokina SA (2013) The role of the Barents Sea in the Arctic climate system. *Rev. Geophys.* 51: 415-449, doi:10.1002/rog.20017.

Smith WO and Sakshaug E (1990) Polar phytoplankton. In: Smith WO (ed) *Polar oceanography, Part B: Chemistry, Biology and Geology*. Academic Press, New York, 447-525.

Sorteberg A and Kvingedal B (2006) Atmospheric forcing on the Barents Sea winter ice extent. *J. Clim.* 19: 4772-4784.

Spielhagen RF and Erlenkeuser H (1994) Stable oxygen and carbon isotopes in planktic foraminifera from the Arctic Ocean surface sediments: Reflection of the low salinity surface water layer. *Mar. Geol.* 119: 227-250.

Spielhagen RF, Werner K, Aagaard-Sørensen S, Zamelczyk K, Kandiano E, Budeus G, Husum K, Marchitto T and Hald M (2011) Enhanced modern heat transfer to the Arctic by warm Atlantic water. *Science* 331: 450-453.

Stangeew E (2001) Distribution and isotopic composition of living planktonic foraminifera N. pachyderma (sinistral) and T. quinqueloba in the high latitude North Atlantic. Ph.D. thesis, Math.-Naturwiss. Fak., Christian-Albrechts-Univ., Kiel, Germany. (Available at http://e-diss.uni-kiel.de/diss_464/pp).

Steinsund PI and Hald M (1994) Recent carbonate dissolution in the Barents Sea: Paleoceanographic applications. *Mar. Geol.* 117: 202-316.

Stuiver M and Reimer PJ (1993) Extended $^{14}C$ data base and revised CALIB 3.0 $^{14}C$ age calibration program. *Radiocarbon* 35: 215-230.

Vinje TE (1977) Sea ice conditions in the European sector of the marginal seas of the Arctic, 1966-75. *Aarb. Nor. Polarinst.* 1975: 163-174.

Vinje T (2001) Anomalies and trends of sea-ice extent and atmospheric circulation in the Nordic Seas during the period 1864-1998. *J. Clim.* 14(3): 255-267.

Volkmann R (2000) Planktic foraminifers in the outer Laptev Sea and the Fram Strait: Modern distribution and ecology. *J. Foramin. Res.* 30: 157-176.

Wanner H, Beer J, Bütikofer J, Crowley TJ, Cubasch U, Flückiger J, Goosse H, Grosjean M, Joos F, Kaplan JO, Küttel M, Müller SA, Prentice C, Solomina O, Stocker TF, Tarasov P, Wagner M and Widmann M (2008) Mid- to Late Holocene climate change: An overview. *Quat. Sci. Rev.* 27(19–20): 791-1828.

Wassmann P, Reigstad M, Haug T, Rudels B, Carroll ML, Hop H, Gabrielsen GW, Falk-Petersen S, Denisenko G, Arashkevich E, Slagstad D and Pavlova O (2006) Food webs and carbon flux in the Barents Sea. *Prog. Oceanogr.* 71: 232-287.

Werner K, Spielhagen RF, Bauch D, Hass HC and Kandiano E (2013) Atlantic Water advection versus sea-ice advances in the eastern Fram Strait during the last 9 ka: Multi proxy evidence for a two-phase Holocene. *Paleoceanography* 28: 283-295.

Wilson LJ, Hald M and Godtliebsen F (2011) Foraminiferal faunal evidence of twentieth-century Barents Sea warming. *Holocene*, 21(4): 527-537.

Yang S and Christensen JH (2012) Arctic sea ice reduction and European cold winters in CMIP5 climate change experiments. *Geophys. Res. Lett.* 39: L20707, doi:10.1029/2012GL053338.

Zamelczyk K, Rasmussen TL, Husum K and Hald M (2013) Marine calcium carbonate preservation vs. climate change over the last two millennia in the Fram Strait: Implications for planktic foraminiferal paleostudies. *Mar. Micropaleontol.* 98: 14-27.

# Figure captions

Table 1: Depth-age model of NP05-11-70GC calibrated using Calib 6.1.1 (Stuiver and Reimer, 1993), the Marine09 calibration curve (Reimer et al., 2009) and a local reservoir age (ΔR) of 105 ± 24 after Mangerud et al. (2006).

Figure 1: The modern oceanography is presented on a bathymetric map of the Barents Sea area. The core location of NP05-11-70GC is indicated by a green circle, whereas previously published records are indicated by number: 1) Risebrobakken et al. (2010) 2) Wilson et al. (2011) 3) Berben et al. (2014) 4) Sarnthein et al. (2003) 5) Rasmussen et al. (2007) 6) Müller et al. (2012); Werner et al. (2013) 7) Skirbekk et al. (2010); Jernas et al. (2013) 8) Müller et al. (2009) 9) Slubowska et al. (2005); Jernas et al. (2013) 10) Klitgaard Kristensen et al. (2013) 11) Lubinski et al. (2001) 12) Duplessy et al. (2001); (2005) 13) Risebrobakken et al. (2011) 14) Duplessy et al. (2005). Northern Barents Sea Opening (NBSO), Barents Sea Opening (BSO), Barents Sea Exit (BSX). A) The main surface currents (Hopkins, 1991). Atlantic water (red): Norwegian Atlantic Current (NwAC), North Cape Current (NCaC), West Spitsbergen Current (WSC), Return Atlantic Current (RAC), Yermak Branch (YB) and Svalbard Branch (SB). Polar water (blue): Bear Island Current (BIC) and East Spitsbergen Current (ESC). Coastal water (black): Norwegian Coastal Current (NCC). B) Seasonal sea ice extent (April (blue) and August (orange)) for the period 1981 – 2010 (National Snow and Ice Data Centre (NSIDC) Boulder Colorado, www.nsidc.com). The observed sea ice extent for April (dotted) and August (dashed) from historical data for four sub periods between 1870 and 2002: 1870 – 1920 (red), 1921 – 1961 (yellow), 1962 – 1988 (pink) and 1989 – 2002 (black) (Divine and Dick, 2006).

Figure 2: Temperature (black) and Salinity (grey) profile at the NP05-11-70GC core site (78.40° N, 32.42° E). Water masses are defined according Gammelsrød et al., 2009.

Figure 3: Depth-age model of NP05-11-70GC. A) Calibrated radiocarbon ages plotted versus depth with a linear interpolation between the dated levels. Error bars indicate the sampled depth intervals and a 2-σ error on the calibrated ages. B) Sedimentation rate versus depth. C) Resolution range versus depth.

Figure 4: Planktic foraminiferal concentration, flux and preservation indicator analysis versus calendar years BP. The black diamonds on the Y-axis denote the AMS $^{14}$C converted to calibrated radiocarbon ages. The in grey highlighted periods are characterized by an increased influence of Atlantic water. A) Total planktic foraminiferal concentration (line) and flux (fill) versus age. B) Planktic foraminiferal fragmentation versus age. C) Mean shell weight of *N. pachyderma* versus age.

Figure 5: Planktic foraminiferal fauna analysis versus calendar years BP. The black diamonds on the Y-axis denote the AMS $^{14}$C converted to calibrated radiocarbon ages. The in grey highlighted periods are characterized by an increased influence of Atlantic water. A) Total planktic foraminiferal concentration (line) and flux (fill) versus age. B-G) Species-specific relative abundance (line) and flux (fill) versus age. H) July insolation at 78° N (Laskar et al., 2004) (note the reversed axis) versus age.

Figure 6: Stable isotopes analysis performed on *N. pachyderma* versus calendar year BP. The black diamonds on the Y-axis denote the AMS $^{14}$C converted to calibrated radiocarbon ages. The in grey highlighted periods are characterized by an increased influence of Atlantic water. A) $\delta^{18}$O measurements corrected for ice volume effect after Fairbanks (1989) versus age. B) $\delta^{13}$C measurements versus age. C) July insolation at 78° N (Laskar et al., 2004) (note the reversed axis) versus age.

Figure 7: Biomarker analysis versus calendar years BP: biomarker-specific fluxes (fill) and concentrations normalized to sediment (black line) and to total organic carbon (grey line). The black diamonds on the Y-axis denote the AMS $^{14}$C converted to calibrated radiocarbon ages. The in grey highlighted periods are characterized by an increased influence of Atlantic water. A) Sea ice biomarker $IP_{25}$ versus age. B) Phytoplankton biomarker brassicasterol versus age. C) Total organic carbon versus age. D) $P_BIP_{25}$ (fill) and July insolation at 78° N (line) (Laskar et al., 2004) (note the reversed axis) versus age.

Figure 8: Scenarios of the proposed biomarker production (scheme) and seasonal sea ice distribution (map) scenarios at the NP05-11-70GC core location (green circle). A-C) Proposed biomarker production and seasonal sea ice distribution scenarios for, respectively, the early Holocene, the mid Holocene and the late Holocene. The shaded areas represent the proposed variability of the sea ice edge whereas the numbers indicate the core locations of previous studies: 1) Berben et al. (2014), 2) Müller et al. (2012), 3) Müller et al. (2009), 4) Klitgaard Kristensen et al. (2013), and 5) Duplessy et a. (2001). D) Present day situation based on mean sea ice extent

(1981 - 2010) for March (black), April (blue) and August (orange) (National Snow and Ice Data Centre (NSIDC) Boulder Colorado, www.nsidc.com).

Table 1

| Lab ID | Core depth (cm) | Material | Uncorrected AMS $^{14}$C age | 1σ | Calibrated age 2-σ range | Calibrated age used in depth-age model (cal yr BP) |
|---|---|---|---|---|---|---|
| Beta-331327 | 47 - 53 | Benthic foraminifera | 2780 | 30 | 2281 - 2496 | 2389 |
| Beta-346803 | 77 - 82 | Benthic foraminifera | 6110 | 40 | 6298 - 6536 | 6417 |
| Beta-331328 | 132 - 137 | Benthic foraminifera | 8870 | 50 | 9307 - 9527 | 9417 |
| Beta-331329 | 223 - 240 | Benthic foraminifera | > 43500 | | | |

Figure 1

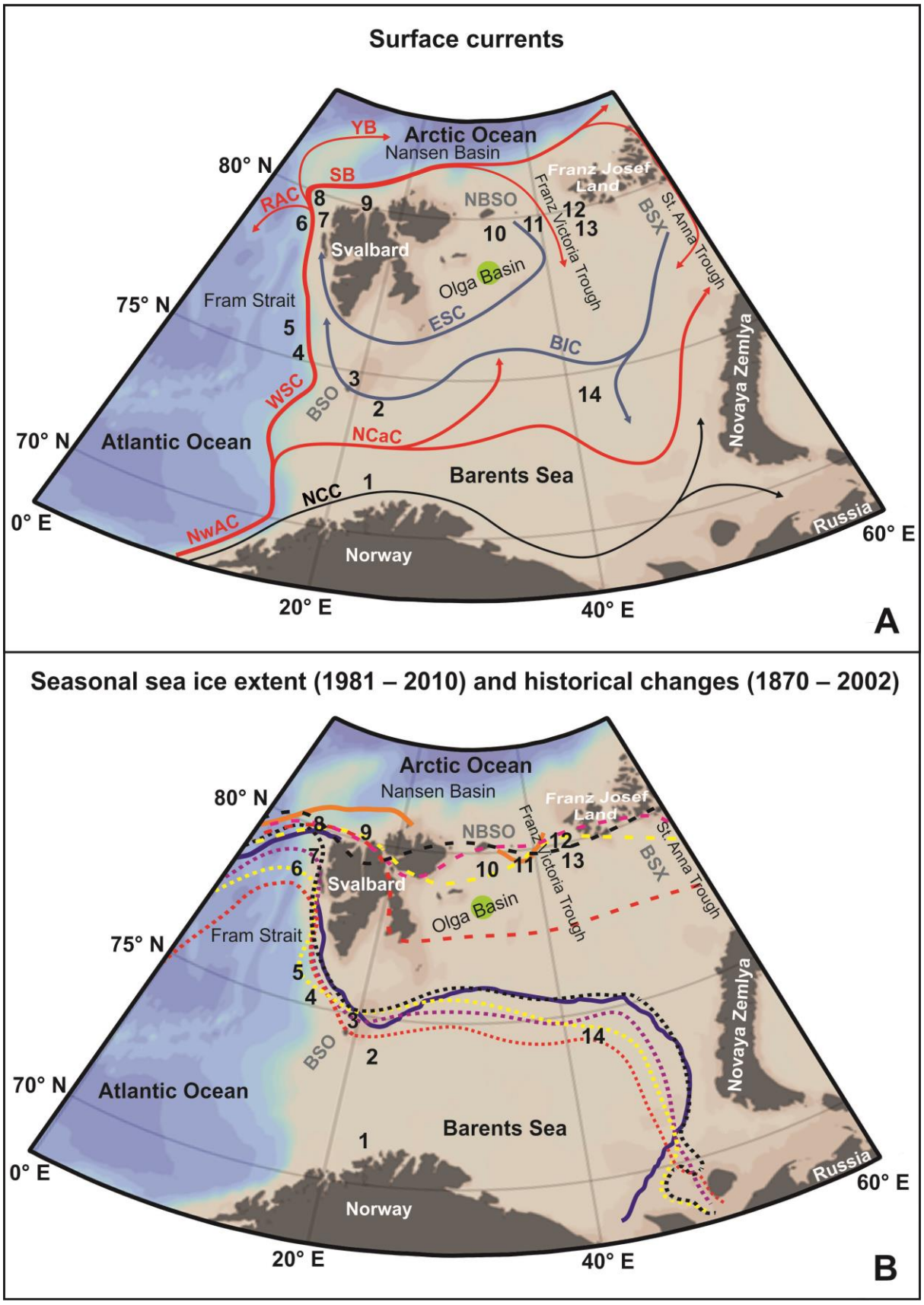
Surface currents
Arctic Ocean
Nansen Basin
YB
SB
RAC
80° N
75° N
70° N
0° E
20° E
40° E
60° E
Fram Strait
Svalbard
NBSO
Franz Victoria Trough
Franz Josef Land
BSX
St. Anna Trough
Olga Basin
ESC
BIC
WSC
BSO
NCaC
NCC
NwAC
Atlantic Ocean
Barents Sea
Norway
Russia
Novaya Zemlya
1
2
3
4
5
6
7
8
9
10
11
12
13
14
A
Seasonal sea ice extent (1981 – 2010) and historical changes (1870 – 2002)
Arctic Ocean
Nansen Basin
80° N
75° N
70° N
0° E
20° E
40° E
60° E
Fram Strait
Svalbard
NBSO
Franz Victoria Trough
Franz Josef Land
BSX
St. Anna Trough
Olga Basin
BSO
Atlantic Ocean
Barents Sea
Norway
Russia
Novaya Zemlya
1
2
3
4
5
6
7
8
9
10
11
12
13
14
B

Figure 2

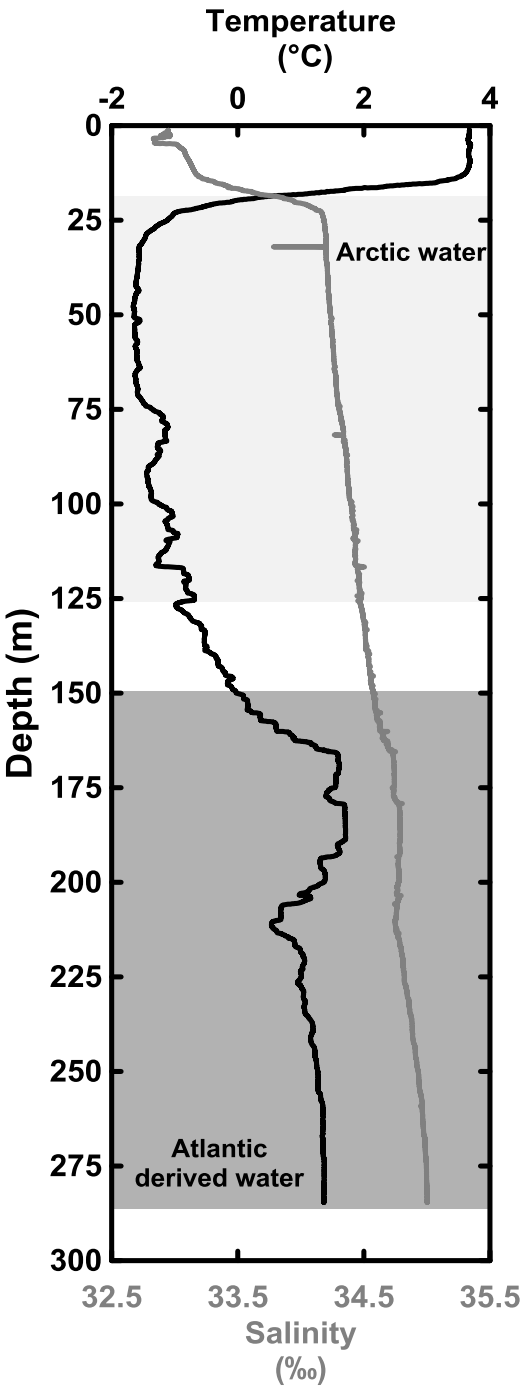
Temperature
(°C)
-2
0
2
4
0
25
50
75
100
125
150
175
200
225
250
275
300
Depth (m)
Arctic water
Atlantic
derived water
32.5
33.5
34.5
35.5
Salinity
(‰)

Figure 3

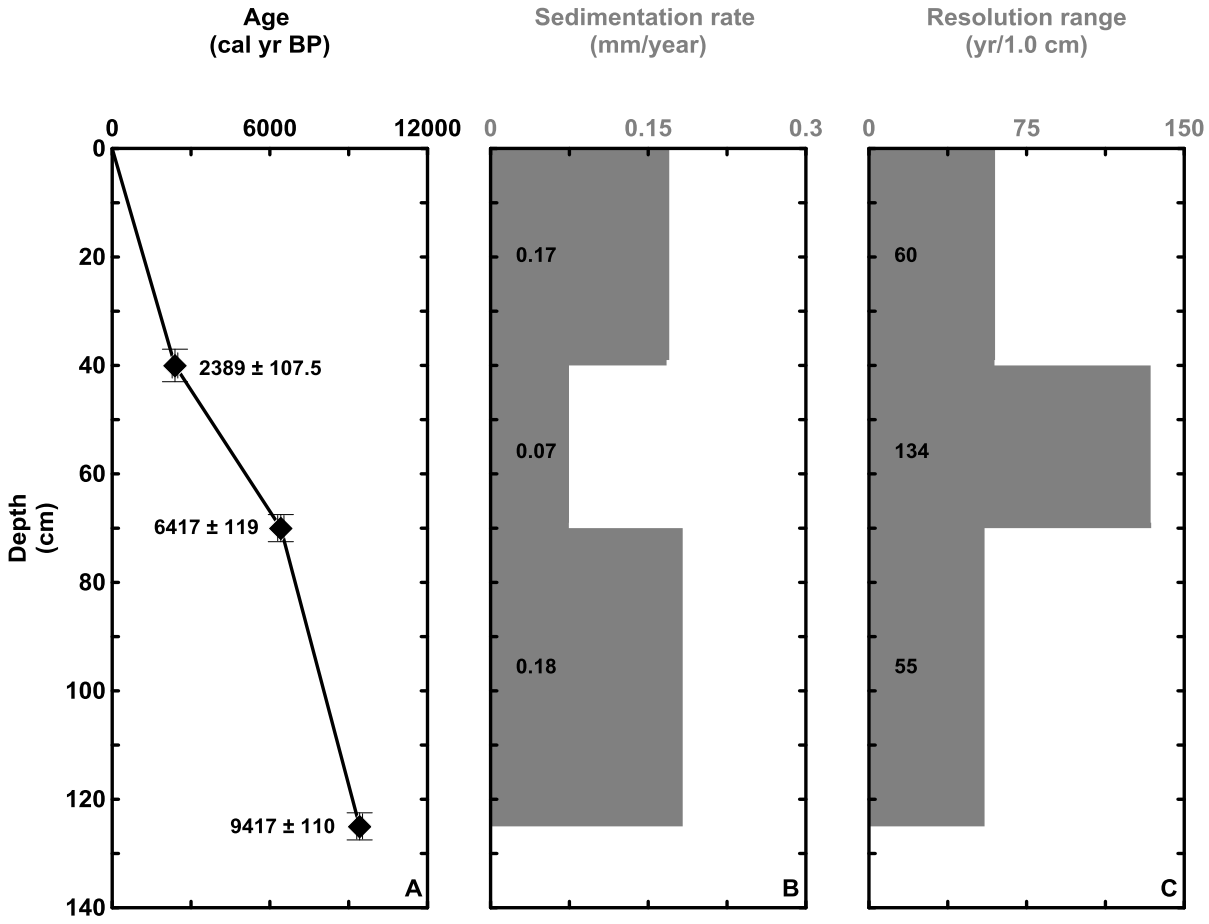
Age
(cal yr BP)
Sedimentation rate
(mm/year)
Resolution range
(yr/1.0 cm)
0
6000
12000
0
0.15
0.3
0
75
150
Depth
(cm)
0
20
40
60
80
100
120
140
2389 ± 107.5
6417 ± 119
9417 ± 110
A
0.17
0.07
0.18
B
60
134
55
C

Figure 4

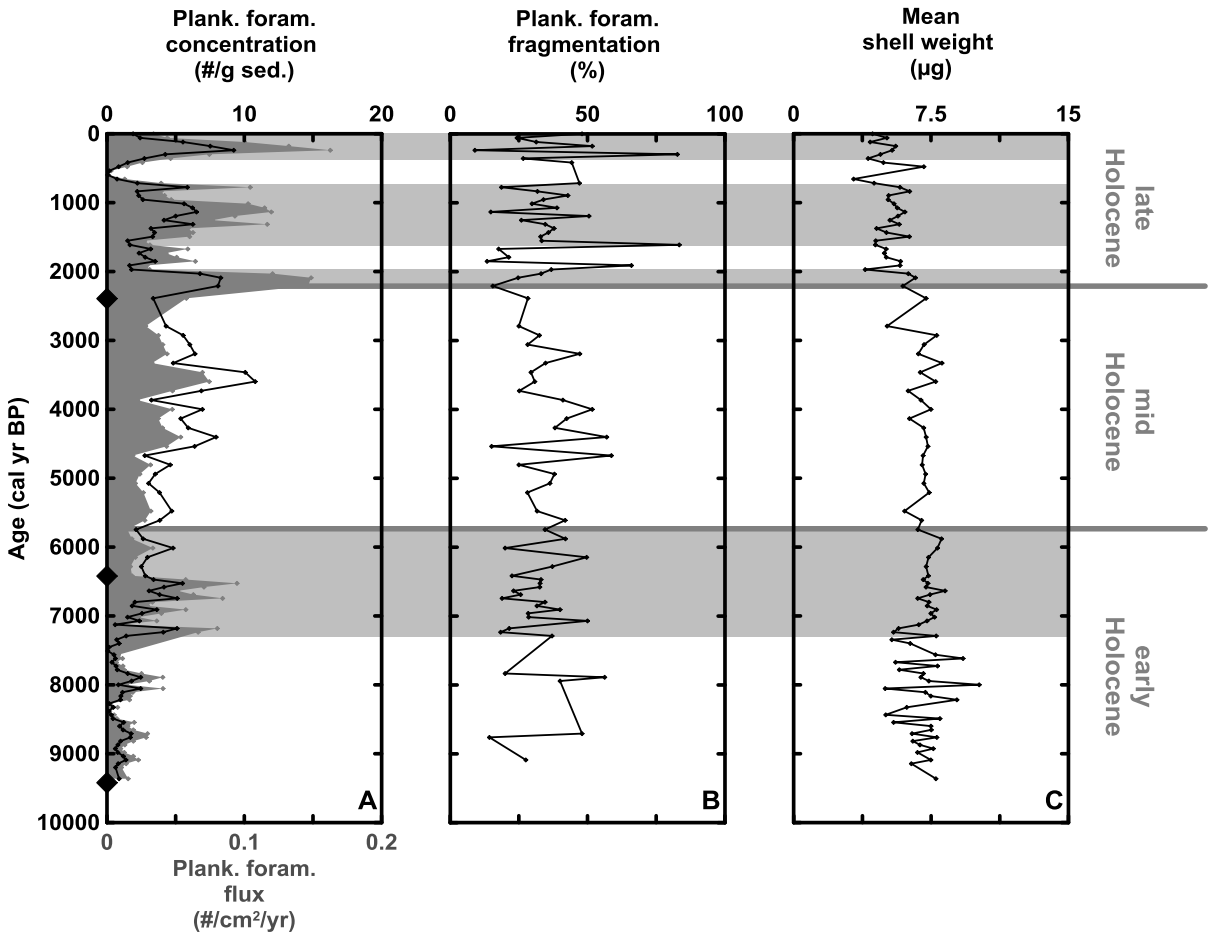
Plank. foram. concentration (#/g sed.)
Plank. foram. fragmentation (%)
Mean shell weight (µg)
0
10
20
50
100
7.5
15
Age (cal yr BP)
0
1000
2000
3000
4000
5000
6000
7000
8000
9000
10000
late Holocene
mid Holocene
early Holocene
A
B
C
0
0.1
0.2
Plank. foram. flux (#/cm²/yr)

Figure 5

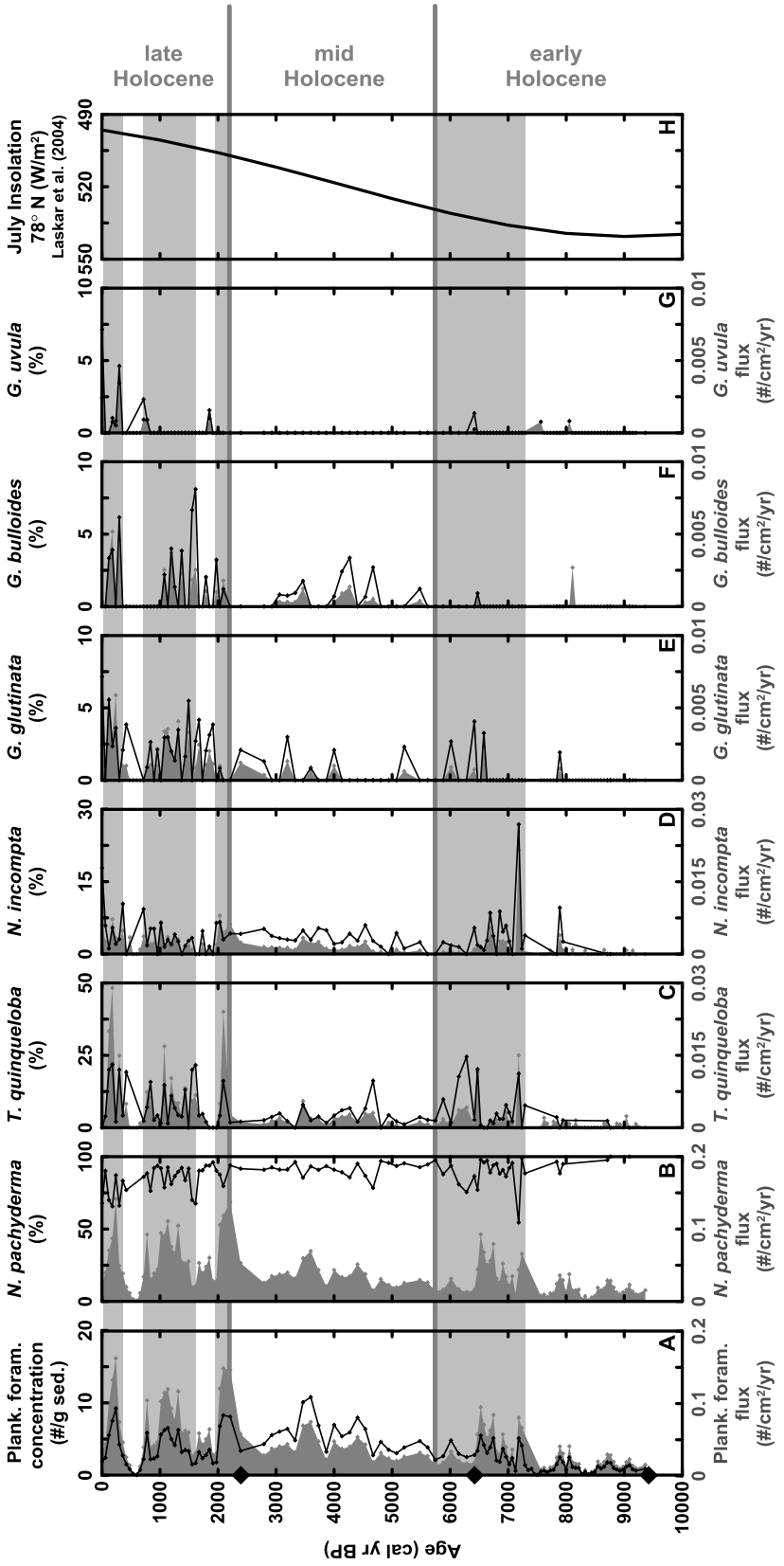
late Holocene
mid Holocene
early Holocene
July Insolation 78° N (W/m²) Laskar et al. (2004)
Plank. foram. concentration (#/g sed.)
N. pachyderma (%)
T. quinqueloba (%)
N. incompta (%)
G. glutinata (%)
G. bulloides (%)
G. uvula (%)
Plank. foram. flux (#/cm²/yr)
N. pachyderma flux (#/cm²/yr)
T. quinqueloba flux (#/cm²/yr)
N. incompta flux (#/cm²/yr)
G. glutinata flux (#/cm²/yr)
G. bulloides flux (#/cm²/yr)
G. uvula flux (#/cm²/yr)
A
B
C
D
E
F
G
H
Age (cal yr BP)

Figure 6

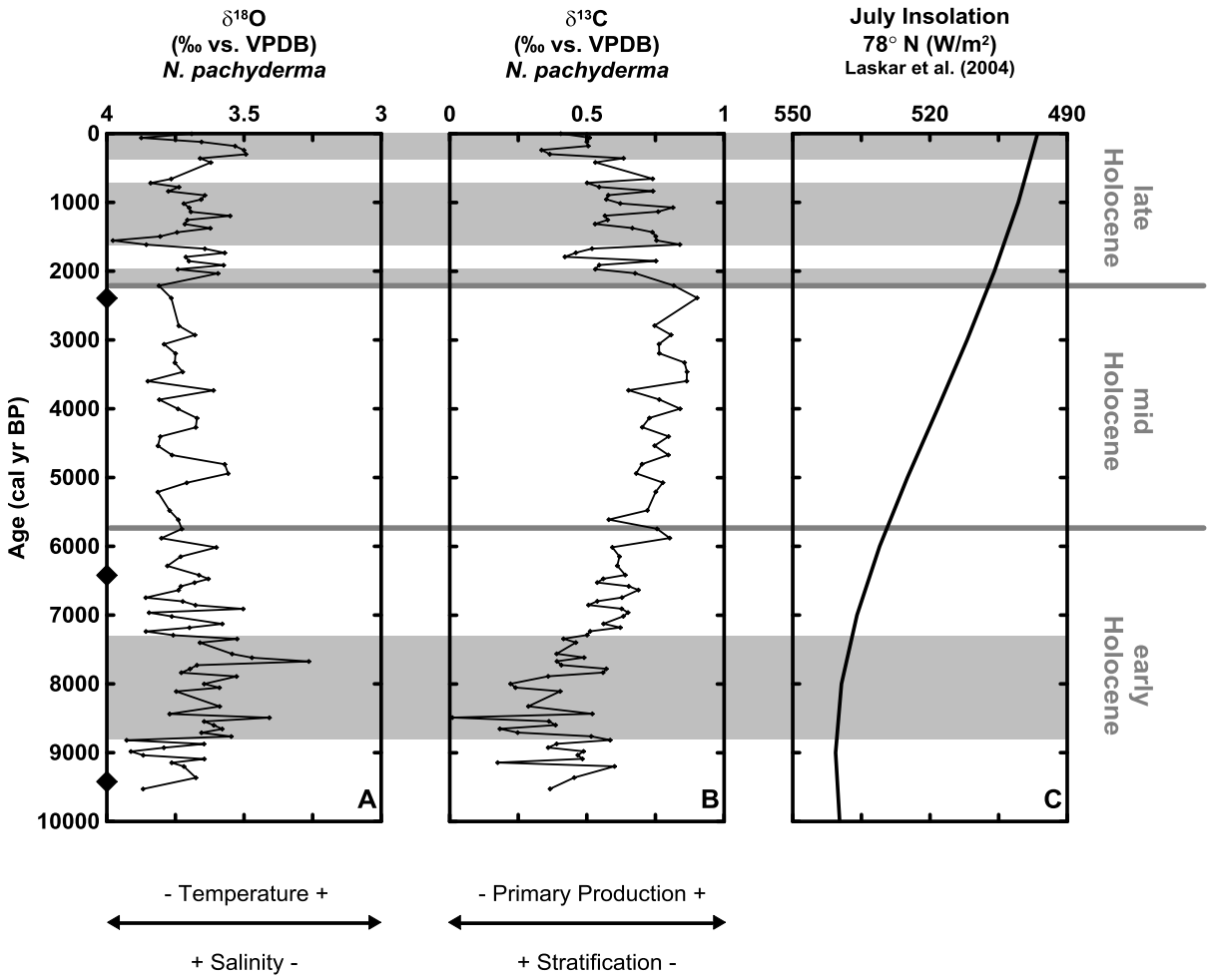
δ18O
(‰ vs. VPDB)
N. pachyderma
δ13C
(‰ vs. VPDB)
N. pachyderma
July Insolation
78° N (W/m2)
Laskar et al. (2004)
4
3.5
3
0
0.5
1
550
520
490
Age (cal yr BP)
0
1000
2000
3000
4000
5000
6000
7000
8000
9000
10000
late Holocene
mid Holocene
early Holocene
A
B
C
- Temperature +
+ Salinity -
- Primary Production +
+ Stratification -

Figure 7

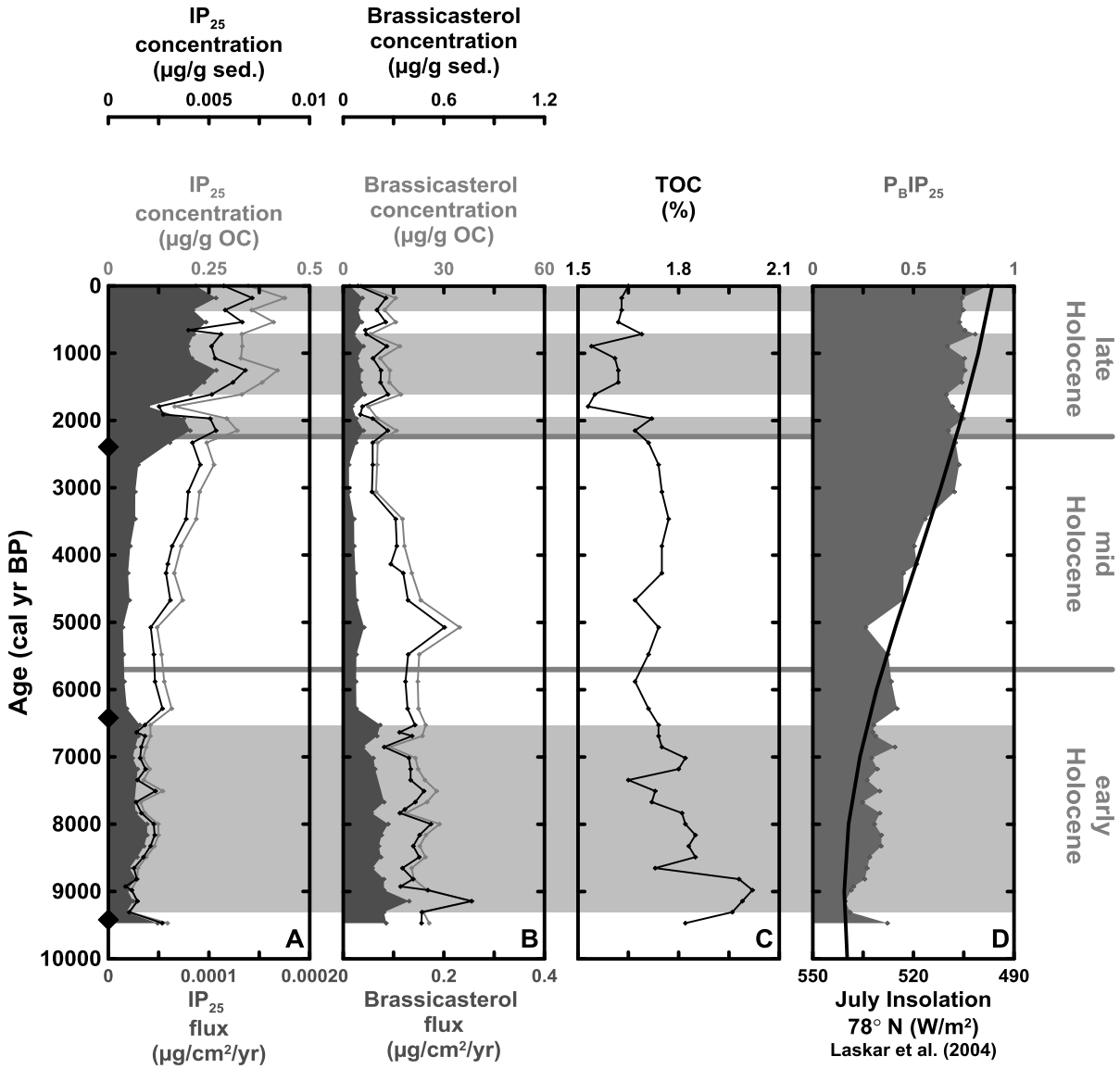
IP25 concentration (µg/g sed.)
0 0.005 0.01
Brassicasterol concentration (µg/g sed.)
0 0.6 1.2
IP25 concentration (µg/g OC)
0 0.25 0.5
Brassicasterol concentration (µg/g OC)
0 30 60
TOC (%)
1.5 1.8 2.1
PBIP25
0 0.5 1
Age (cal yr BP)
0 1000 2000 3000 4000 5000 6000 7000 8000 9000 10000
late Holocene
mid Holocene
early Holocene
A
B
C
D
0 0.0001 0.00020
IP25 flux (µg/cm²/yr)
0 0.2 0.4
Brassicasterol flux (µg/cm²/yr)
550 520 490
July Insolation 78° N (W/m²)
Laskar et al. (2004)

Figure 8

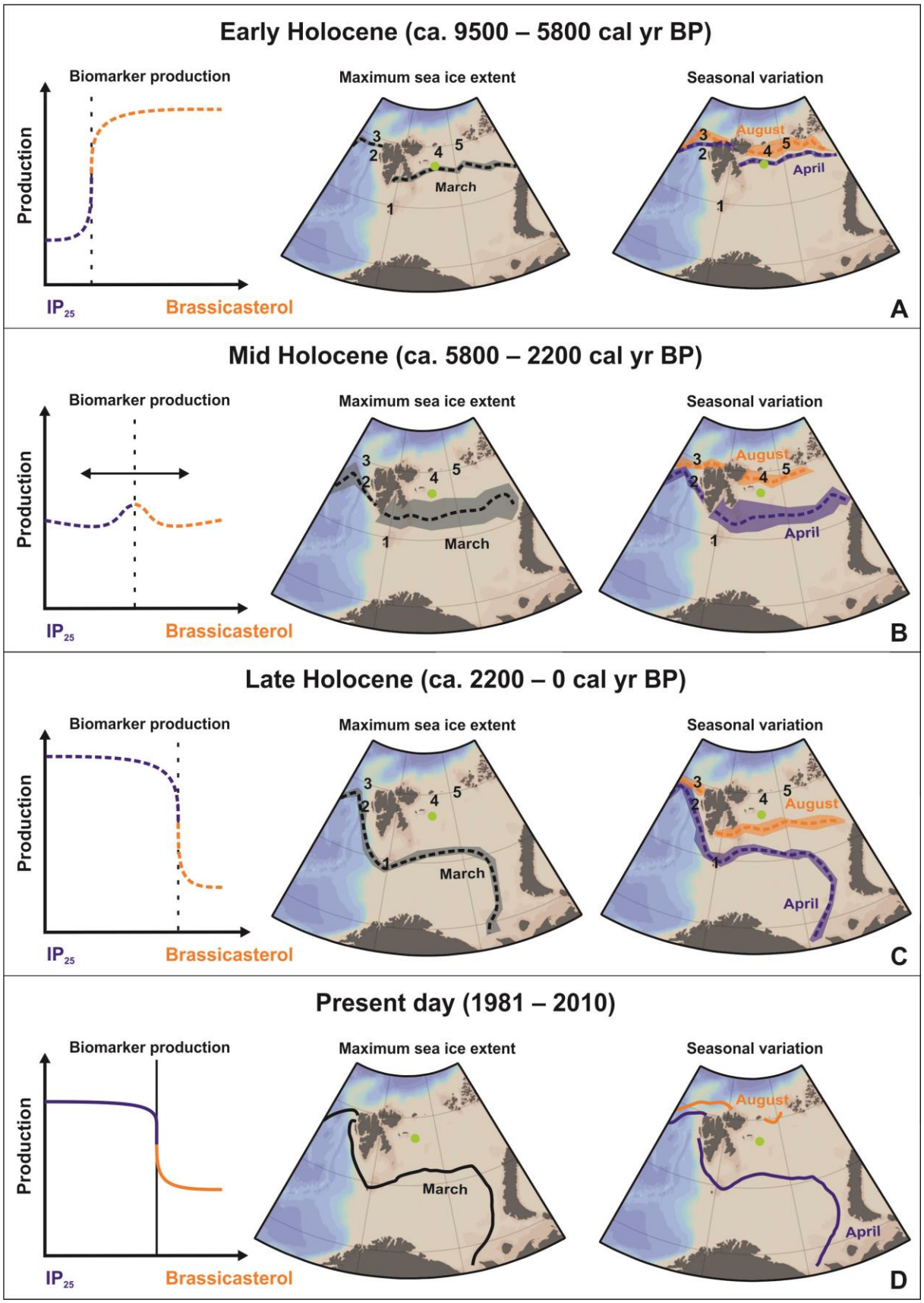
Early Holocene (ca. 9500 – 5800 cal yr BP)
Biomarker production
Production
IP25
Brassicasterol
Maximum sea ice extent
Seasonal variation
August
April
March
1
2
3
4
5
A
Mid Holocene (ca. 5800 – 2200 cal yr BP)
Biomarker production
Production
IP25
Brassicasterol
Maximum sea ice extent
Seasonal variation
August
April
March
1
2
3
4
5
B
Late Holocene (ca. 2200 – 0 cal yr BP)
Biomarker production
Production
IP25
Brassicasterol
Maximum sea ice extent
Seasonal variation
August
April
March
1
2
3
4
5
C
Present day (1981 – 2010)
Biomarker production
Production
IP25
Brassicasterol
Maximum sea ice extent
Seasonal variation
August
April
March
D